AD-A189 205 DEEP WATER MASS CIRCULATION IN THE ALBORAN BASIN MEASUREMENTS - JANUARY T..(U) SACLANT ASW RESEARCH CENTRE LA SPEZIA (ITALY) P PISTEK SEP 87 1/1

UNCLASSIFIED SACLANTCEN-SM-195 F/G 8/3 NL

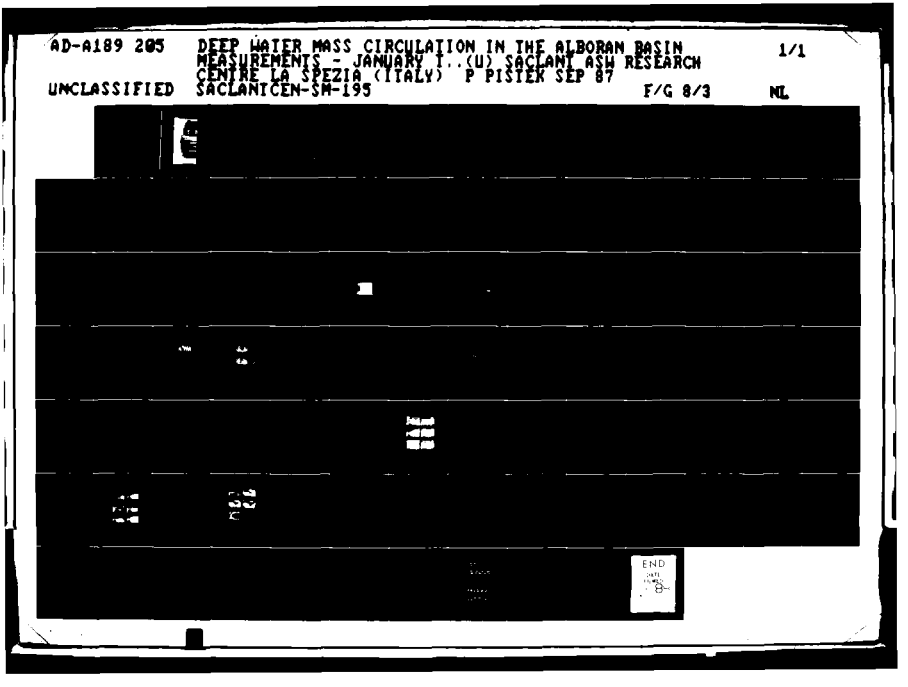

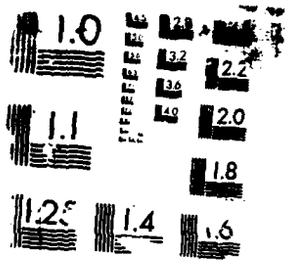

MICROCOPY RESOLUTION TEST CHART

(4)

OTIC FILE COPY

SACLANT
RESEARC
MEMORAN

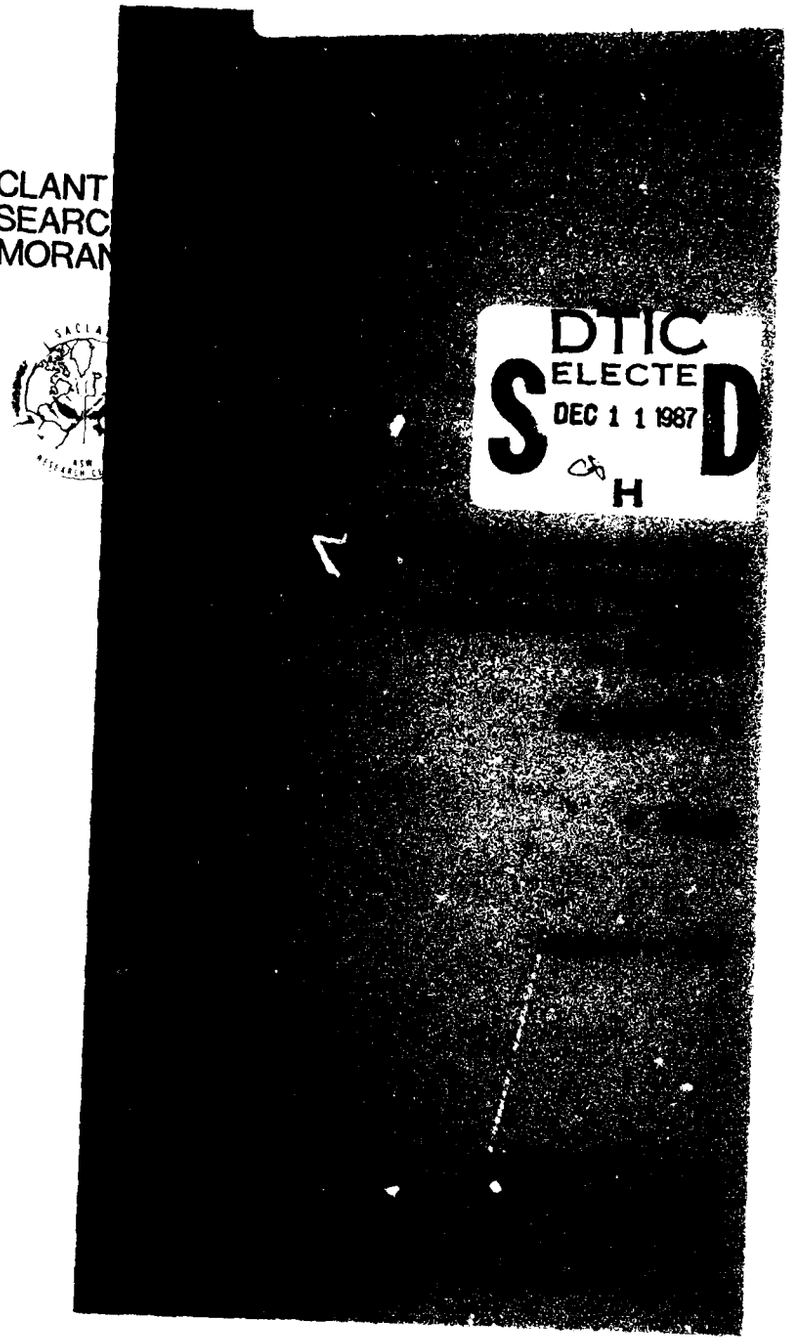

87 52

Page count for SM-195
(excluding covers)

Pages	Total
i–vi	6
1–23	23
@1–@60	60
	89

SAC'LANT ASW Research Centre
Viale San Bartolomeo 400
19026 San Bartolomeo (SP), Italy

tel: 0187 540 111
telex: 271148 SAC'ENT I

NORTH ATLANTIC TREATY ORGANIZATION

SACLANTCEN SM-195

Deep water mass circulation in the Alboran basin: Measurements – January to April '82

ALBORAN II

P. Pistek

The content of this document pertains to work performed under Project 04 of the SACLANTCEN Programme of Work. The document has been approved for release by The Director, SACLANTCEN.

Issued by:
Underwater Research Division

Rolf Thiele

R. Thiele
Division Chief

intentionally blank page

Deep water mass circulation in the Alboran basin: Measurements – January to April '82

ALBORAN II

P. Pistek

Abstract: Alboran Sea circulation between 220 m and 1100 m depth is studied. Interactions between three water types, Atlantic water, Levantine water, and western Mediterranean Deep water cause a complicated flow pattern. Atlantic water flowing as a jet through the Strait of Gibraltar forms a variable anticyclonic gyre down to a depth of 200 m. A few works based on geostrophic calculations and the Bernoulli equation treat the deep flow. The measurements by moored current meters and free-floating vertical current meters deployed and acoustically tracked in the western part of the Moroccan continental slope revealed an enhanced current along this slope toward Gibraltar. The study of the total deep circulation pattern in the Alboran basin used a combination of current meter and free float measurements. The tracks of the floats at all depths from 220 m to 1100 m revealed broad and slow (approx. 2.5 cm/s) cyclonic circulation located under the surface anticyclonic gyre. Floats revealed the boundary current along the Moroccan continental slope to have a more complicated pattern, moving eastward or westward after reaching the slope east or west of 4.0°W respectively.

Current-meter data generally agreed with these results. The time-dependent vector field of currents created from all of the float and current-meter readings shows periods of enhanced and extended cyclonic motion followed by stagnation and even reversal of current direction in external positions, with only the small cyclonic vortex. The satellite and conductivity-temperature-depth (CTD) data indicated the existence of an anticyclonic gyre with variable extension into the south-western part of the Alboran during the experiments. Considerable upward bending of isolines across the Moroccan continental slope was visible, but the lateral extension and the depth of the anticyclonic circulation do not agree with the existing explanation in the literature. Integrated atmospheric pressure over the western Mediterranean and the Alboran Sea did not correlate with the currents.

Keywords: Alboran Basin o Alboran Sea o anticyclonic motion o Atlantic o Bernoulli equation circulation o currents o cyclonic motion o free-floating vertical current meters o geostrophic o gyre o Levantine o Mediterranean o moored current meters o Moroccan continental slope o Strait of Gibraltar

intentionally blank page

Preface

The SACLANT Applied Oceanography Group conducted several intensive oceanographic investigations in the Alboran Sea during 1980-82.

This strategically important area has a complicated and variable oceanographic structure with strong thermal fronts, eddies, and jets, and large variations in salinity. The purpose of the cruises was to obtain the oceanographic data which would help to describe and understand the oceanographic features and ultimately serve as input and 'truth' data for numerical models of the Alboran Sea circulation.

Three sets of cruises were conducted:

(a) ALBORAN I, two cruises in 1980;
(b) ALBORAN II, three cruises in the winter 1982;
(c) ALBORAN III, two cruises in the summer-fall 1983.

The results of the 1980 cruises have been described by P. Pistek (1984). The present report treats the results of ALBORAN II. The main purpose of this set of measurements was the description of the deep Alboran Sea circulation in winter using the Lagrangian technique. For this purpose, Swallow-type floats were deployed and acoustically tracked from moored listening stations.

SACLANTCEN devoted considerable effort and resources to developing the Lagrangian technique. The Centre's Ocean Engineering Department redesigned and built the floats, developed the acoustic releaser and added the pressure sensor. All testing and development for the deployment and recovery of the system was done at the Centre. Listening stations were developed by A. Bradley (Woods Hole Oceanographic Inst.) and P. Tillier (Centre Océanologique de Bretagne, Brest), and built in Brest, France.

Contents

1. Introduction

The Mediterannean is an area where evaporation greatly exceeds precipitation and river runoff. The major connection with the outside ocean is through the Strait of Gibraltar. To achieve a mass balance, the net inflow from the Atlantic is required. A salt balance, and observed salinities in the Atlantic and the Mediterranean, requires that the net flux arises from the difference between a surface inflow and bottom outflow, each about twenty times larger than the net flow. This problem has already been treated by Defant (1961) and Deacon (1971). Also, Lacombe (1961) and Lacombe et al (1964) arrived at values for the fluxes about 25% smaller than the figures given by Bethoux (1980), whose 53×10^{12} m^3/yr for inflow and 50.5×10^{12} m^3/yr for outflow were obtained by considering all of the budgets for the Mediterranean; however, neither of these estimates is definitive.

The circulation in the Alboran Sea, which is in the vicinity of the Strait, is strongly influenced by this exchange, and on the seasonal timescale the current fluctuations in the Strait of Gibraltar may be associated with the seasonal cycle of evaporation minus precipitation for the Mediterranean, or with seasonal changes in water stratification.

In this context the measurements of Lacombe et al (1964) showed that although the mean flow, tidal currents and sub-tidal flows have considerable spatial variability, currents of the order of 0.5 to 1 $m\,s^{-1}$ are representative of all three types of flow through the Strait of Gibraltar.

However, there are current fluctuations with periods of days to months, but these are most likely to be associated with meteorological forcing, because the Atlantic and the Mediterranean respond to large-scale patterns of atmospheric pressure and wind. As the Atlantic is large the atmospheric pressure effects are rapidly equilibriated, but the Mediterranean has only a single connection, the Strait of Gibraltar, to the Atlantic Ocean, and so one would expect significant flows through the Strait to occur in response to changes in the average atmospheric pressure over the Mediterranean.

This problem was investigated in more detail by Lacombe et al (1964) and Crepon (1965). Crepon found the fluctuations of sea level are inversely correlated to the atmospheric pressure. He also found the sea level difference between the south and north sides of the Strait of Gibraltar, representing surface inflow, to be inversely correlated to the average atmospheric pressure over the Western Mediterranean. As recognized by Lacombe et al (1964) and Crepon (1965), this appears to be contrary to simple requirements of mass conservation, which would require the rate of change of sea level in the Mediterranean, rather than the sea level itself, to

be correlated with the inflow. Garrett (1983) discussed as a possible solution the significant fluctuations in the flow through the Strait of Sicily.

Another manifestation of the meteorological forcing is the wind-driven change in deep currents caused by wind-driven set-up. However, as most of the Mediterranean is relatively deep it is suggested that the basin-average changes in sea level due to wind, and the associated flows, will not be large. There remains the possibility that significant wind-driven set-ups in the vicinity of the Strait of Gibraltar considerably influence the flow through the Strait and changes in mean sea level, but as shown by Garrett (1983) the influence of the wind driven set-ups appears to be less important than atmospheric pressure, at least for periods of around 10 days and longer. Garrett (1983) estimates the ratio of sea level changes due to wind to that of pressure to be about 0.3 for the 10-day periodicity. If there is a barotropic response to atmospheric pressure forcing the current variation should be detectable in the Alboran because the ratio of the cross-sectional area of the Strait of Gibraltar to that of the Alboran indicates the appropriate barotropic current changes (of the order of a few cm/s in the Alboran: part of this report is concerned with the correlation of the atmospheric pressure and deep currents in the Alboran Sea).

The circulation in the western Alboran basin involves both Atlantic and Mediterranean waters. The three types of water considered, as identified by Briden and Stommel (1982), are: Atlantic Water, Levantine Water, and Western Mediterranean Deep Water. The Atlantic Water forms the inflow to the Alboran Sea, and the Levantine and Western Mediterranean Deep Waters comprise the outflow of Mediterranean water through the Alboran Sea and the Strait of Gibraltar into the Atlantic. Atlantic Water forms a top layer about 150 m thick that flows into the Alboran Sea from the Atlantic as a 20 km wide jet at a speed of several km/h. Its characteristic salinity is 36.5 and its temperature is seasonal. This energetic layer creates anticyclonic circulation in the south-western part of the Alboran. Its extension and depth are quite variable. It is documented by Ovchinnikov et al (1962), Lacombe (1971), Lanoix (1974), Cheney and Doblar (1978), Bucca and Kinder (1984), and by participants of the 'DONDE VA' experiment (Parilla, 1984). Laboratory modelling has been reported by Whitehead and Miller (1979). This anticyclonic circulation is clearly visible on the satellite infrared images of the sea-surface temperature, as shown by Wannamaker (1979), Philippe and Harang (1982) and La Violette (1983). Numerical studies of the upper layer circulation in the Alboran Sea done by Preller (1981) and Preller and Hurlburt (1982) showed the strong influence of the vorticity input and velocity amplitude of the inflow through the Strait of Gibraltar on the extension and location of the anticyclonic gyre. The forcing mechanism for the change of these parameters is not clearly understood. An earlier explanation that the gyre and its changes are forced by anomalies in the wind fields was shown to be incorrect (Whitehead and Miller, 1979). Cheney and Doblar (1978) observed that the low pressure over the western Mediterranean in conjunction with a westerly wind caused the migration of the gyre to the east, while the opposite conditions favored the development of a large gyre in the western

Alboran. Several observations which agree with the Cheney and Doblar hypothesis, and some which do not agree, are described in this report.

Under the 150 m thick surface layer there is water of Mediterranean origin. Uppermost is the intermediate Levantine Water formed near Rhodes (Ozturgut, 1976) and characterized throughout the Mediterranean by a mid-depth maximum in both temperature and salinity (Wust, 1961). The western Mediterranean Deep Water formed south of France (MEDOC Group, 1970) is deeper, less saline, and cooler, with a potential density of 29.10 kg/m^3 or greater and a potential temperature of less than 12.90 °C (Sankey, 1973; Stommel, 1972).

Stommel et al (1973), Porter (1976), Bryden and Stommel (1982), Pistek (1984), and Kinder (1984) have addressed the deep flow. Bryden and Stommel (1982) obtained the enhanced flow near the southern boundary from geostrophic calculations; their current meter data from one mooring showed a current directed along the Moroccan continental slope towards Gibraltar, with small seasonal variability; Kinder's (1984) current meter data taken in the northern Alboran showed slow ($\sim$ 1 cm/s) southwesterly flow at 500 m and very sluggish easterly flow at >500 m. Current meter and free floating vertical current meter data obtained in 1980 (Pistek, 1984), also indicated the slow flow in the center of the Alboran Sea, with a westerly direction for the intermediate water, a changeable direction for the deep water, and an enhanced and accelerated flow along the Moroccan continental slope towards Gibraltar.

Relative contributions of the Levantine and Deep Western Mediterranean Waters to the outflow of Mediterranean Water through the Strait of Gibraltar are important parameters for Mediterranean circulation. It is in the Alboran Sea that the proportions of the different water masses in this outflow are established. Hence the knowledge of the deep flow pattern, its time variability, and its eventual coupling with the upper layer are important for understanding the mixing and its dynamics. The main purpose of the present work was to investigate the general pattern of deep circulation by deploying the set of current-meter moorings and by tracking the Swallow-type floats and simultaneously observing the upper-layer variability.

2. Equipment and experimental procedure

Acoustically-tracked free floats (Swallow-type) were used in the Lagrangian description of circulation. Acoustic tracking was done from three moored listening stations; their design is described by Tillier (1980) and Bradly and Tillier (1980).

The original float design was considerably modified at SACLANTCEN. The small glass sphere used for the float's electronics was replaced by one with a 50 cm diameter. A pressure transducer and releaser were added, and a flash and a radio transmitter were mounted on each float to help locate them on the surface. Because the in-situ density change in the Alboran, deeper than 200 m, is essentially only due to compression, to position the floats in the range of ± 25 m from the desired deployment depth requires a precision is of the order of $2 \times 10^{-5} g/cm^3$ in establishing the float density in air. The methodology for measuring the float density precisely is described in Pistek, de Strobel, Montanari (1984). The compressibility of the glass sphere was established from the Benthos buoyancy data, but the large error introduced by non-linear compression of 'rubber' parts of the float (cables, sealing material) was eliminated empirically by standardisation of these parts and by developing the empirical curve of the float's density in the air versus the depth dependence after many deployments. For this purpose the small electromagnetic releaser mounted outside the float was very useful: it was activated by acoustical command from the ship at a frequency of 10 kHz by a signal transmitted by the EG&G system and released the 2 kg of ballast which caused the float to ascend. A schematic and photograph of the float is given as Fig. 1.

Floats were tracked automatically from three autonomous listening stations (ALS). Figure 2 shows the schematic. Each ALS was composed of a hydrophone array (4 hydrophones), an amplifier, and a microprocessor with a correlator and a tape recorder. The amplifier had automatic gain control and amplified each received signal to the same level; thereafter the amplitude information was lost in processing and only the phase was utilized. A heterodyne mixer changed the frequencies from the range of 1562.5–1572.5 Hz to 1–10 Hz and this signal formed the input to the microprocessor. Every 4 min the pinger on each station transmitted the latest information about correlation from the memory register of the microprocessor. The signal was received by the ship's echo sounder at 5 kHz. In this way it was possible to check the proper functioning of the ALS after deployment.

The floats used for the 1982 experiment consisted of glass spheres with cylindrical pressure transducers hanging beneath; the electronics were housed inside. Some of the floats had an electromagnetic releaser and all of them transmitted at two-hour intervals; the signal lasted 20 s in a frequency sweep from 1562.5 Hz to 1572.5 Hz. During the first four successive transmissions (8 h) information about depth was

transmitted as a repetitive signal, with the delay of the second signal being proportional to the depth. Three moored ALS were positioned at 400 m depth to track the floats. Each station sampled the acoustic environment every 25 ms and cross-correlated the received signal with the standard signal stored in the memory of its microprocessor. The four highest cross-correlations in each 4-min interval were stored, together with corresponding times, on magnetic tape.

All of the floats and listening stations were synchronized. Transmissions from different floats were separated by a 10-min interval. Because the delay in arrival time is proportional to the distance of the float from the station, triangulation from three stations positioned the float every two hours.

One of the listening stations was located on the ship. An acoustic array and amplifier were mounted on a Sv Grundy TDS system whose sound speed channel was used to transmit acoustic measurements. Both TDS measurements and acoustic listening were performed with this arrangement. In the later measurements the TDS system was replaced by a N. Brown CTD MK III system. The station was equipped with a printer instead of a magnetic-tape recorder, and every 4 min it printed and plotted the four highest correlations and the time. After the measurements were finished, the floats were located from the ship with the help of the shipborne receiver; a release on the floats is triggent to let acoustically released to let them rise to the surface for collection; a radio transmitter and a floating light mounted on each float helped to locate them on the sea surface. The tracking procedure is shown in Fig. 3.

Six subsurface moorings, each with two attendant current meters, were deployed in the Alboran Sea. Three of the moorings had an ALS station. The mooring links were made of Kevlar and there was an EG&G transponder and a releaser; the buoyancy (glass spheres) was distributed uniformly along the mooring line, with the shallowest part at 280 m. Figure 4 is a schematic of the configuration. Ten current meters were of the propeller type and two were of the 2-axis N. Brown acoustic type. The mooring positions are presented in Fig. 5; three current meters were deployed on mooring G but the deepest one (at 1300 m) failed.

3. Measurements and data treatment

3.1. OBJECTIVE

The three cruises described in this report were carried out in January, March and April 1982. Their main objective was to determine the Deep Water circulation pattern in the Alboran Basin, with the aid of floats and current meters. Two current meters were hung on each of six moorings (A, B, C, D, E and F) at depths corresponding to the Levantine and Western Mediterranean Deep Water. In addition autonomous listening stations were attached to three mooring stations (A, B, C). The instruments operated in the period between the end of January and the beginning of May in 1982. Nine floats were released between the end of January and the beginning of May 1982. The positions and periods of deployment of the floats and the current meters are given in Fig. 5. The moorings with the autonomous listening stations (A, B, C) were deployed in deep water to provide acoustic tracking of the floats; moorings E and F were used to investigate the currents in the western part of the Alboran; mooring G was used to measure inflow from the east through the deep channel near Alboran Island. Deployment positions for the first set of floats (1,2,4,5,9) were selected on the basis of 1980 current measurements (Pistek, 1984). Positions for deploying a second set of floats (3,6,7,8) $1\,^1/_2$ months later were selected after the rather unexpected movement of the first set, in order to check the current stability and to provide more details on the central Alboran and along the Moroccan continental slope. The conductivity-temperature-depth (CTD) measurements were made during 3 different periods. (These are also indicated in Figure 5). The locations of the CTD casts are indicated in Fig. 6.

3.2. DATA RECORDING AND PREPARATION

In preparation for analysis, data from the moored instruments were recorded on magnetic tape cassettes, transcribed on to HP 8-track tapes, transferred to UNIVAC disc storage, and purged of bad data.

XBT and CTD data were acquired with the aid of SACLANTCEN's integrated oceanographic system (IOS), which uses a Hewlett-Packard 21MX computer. Data were stored on HP 8-track tapes and later transferred to UNIVAC disc storage where they were cleaned by the removal of spikes and bad profiles.

On-board aquisition of satellite data was performed on a special satellite aquisition system connected to the IOS HP 21MX computer, with data display on line printer or Lexidata image processor and monitor for colour imagery. The data were

stored on an HP 800 bpi magnetic tape and later processed in the SACLANTCEN facilities. The resolution of the satellite APT images is 4 × 4 km.

3.3. FLOATS AND AUTONOMOUS LISTENING STATIONS (ALS)

The floats transmitted their positions every two hours. Precision of float positioning depends on the accurate location of the moored listening stations, the accuracy of the synchronization, electronic drift of the clocks in the floats and stations, the multipath propagation of the sound (possibly involving reflections), and the sharpness of the cross-correlation. The positions of the three moored listening stations were established by radar and satellite navigation with an error of less than 1 km, which established the error in absolute positioning of the float tracks. Before deployment, each instrument was synchronized to within 1 ms by 5 MHz radio signals (from the Istituto Elettrotecnico Nazionale Galileo Ferraris, Torino, Italy.) The drift of the oscillators was much smaller than specified by the manufacturer and was taken into account in the computation of distance. The random variation of the oscillator was less than 2 ms/h. The frequency bandwith allowed the acoustic arrival time to be established to an accuracy of 0.1 s.

Influences of multipath propagation and reflection were sometimes visible as a broadening of the cross-correlation, but they are hard to evaluate because the bottom topography in the Alboran Basin is variable. The average propagation path was about 60 km long and the triangulation was mostly good, with a final precision of about 250 m.

The float-position data (one point every 2 h) were recomputed into average 2-hourly velocities and linearly interpolated to hourly values. A Groves filter (1955) was used to remove tidal effects selectively and as a low-pass filter; only the variations of periodicity greater than $1\,^1/_2$ days were preserved after filtration. Examples of a float's path plotted from raw data and from the data after filtration are given in Pistek (1984)—Fig. 7. Tides and inertial oscillations are visible in the original track but recorded positions of floats were not precise enough to resolve them completely.

3.4. CURRENT METERS

Table 1 summarizes all 12 current-meter measurements The original sampling interval for most of the current meters was 15 min except for the N. Brown and Weller types, both of which used 4 min sampling. Deep currents in the Alboran Sea are very slow. All propeller-type current meters have a threshold higher than 1 cm/s. There were prolonged periods of measurements (namely at position C) when currents (even tidal) were under this threshold. The large vane on N. Brown current meters permits the precise measurement of phase even for current speeds lower than 1 cm/s and no amplitude information.

TABLE 1
Description of current meter data

Mooring	Current-meter[1]	Deployment depth (m)	Data (Julian days)[2] start	Data (Julian days)[2] end	Original sampling (min)	Average velocity (cm/s)	Notes
A	NBA	326	26d 16h 33m	114d 6h 33m	15	1.44	
	NB acoustic	793	26d 16h 44m	114d 7h 44m	4	2.57	
B	NBA	331	23d 18h 29m	114d 13h 29m	15	1.56	from day 87 only the
	NB acoustic	763	23d 18h 19m	114d 13h 43m	4	4.62	phase information
C	NBA	350	24d 17h 16m	113d 13h 16m	15	0.83	
	Weller	725	24d 17h 14m	113d 9h 14m	4	0.77	
E	VACM	385	28d 9h 6m	113d 8h 6m	15	2.87	
	VACM	638	28d 9h 7m	113d 8h 7m	15	2.05	
F	NBA	296	25d 16h 20m	113d 4h 20m	15	1.63	from day 46 only the
	VACM	740	25d 16h 35m	113d 4h 35m	15	1.7	phase information
G	NBA	228	22d 14h 55m	112d 4h 55m	15	3.54	
	NBA	412	22d 14h 57m	112d 4h 57m	15	3.48	

[1] NBA - current meter (N. Brown); VACM EG&G - vector averaging current meter; Weller - propeller type current meter (two propellers in horizontal directions); NB acoustic - N. Brown acoustic current meter.
[2] d, Julian day; h, hour; m, minute.

Original data were filtered by low-pass filter after removing the spikes, then decimated to hourly values; they are presented the Groves filter (1955) used for the float data was applied. Examples of hourly values and filtered current meter data are given in Fig. 20; the spectral effect is shown in Pistek (1984). The non-filtered hourly current meter data show mainly semidiurnal tidal variations; they appear as spikes in Fig. 20.

3.5. HYDROGRAPHY

Short surveys were made with a N. Brown (CTD) in each cruise. Only a small amount of data was taken because of the lack of time. The CTD sensor was calibrated at SACLANTCEN in January, before the cruises, and was recalibrated in March and July. We found considerable drift (0.04) in the salinity measurements for the April casts. The drift was revealed by comparing the salinity/potential-temperature plots with the January casts in such a way that the slopes of Western Mediterranean Deep Water were matched without shifting the potential temperature. Data from every cast were ordered progressively with depth (no return loops

permitted) and the other variables computed. Salinity and potential temperature data variations were averaged to 10 m depth intervals.

3.6. ATMOSPHERIC PRESSURE

The average atmospheric pressure over the Alboran Sea is called ALBORAN in this report and the corresponding Western Mediterranean pressure is called WESTMED. The ALBORAN and WESTMED were evaluated from weather maps of the European Meteorological Bulletin, (D6050 Oftenbach am Main, Frankfurter Strasse 135, Germany) every 12 h for the period of 130 days (Julian days 7 to 137) overlapping the period of measurements. Average atmospheric pressure was obtained by integrating the area between each two isobars on the meteorological map by planimeter, multiplying the resulting area by average pressure for each strip, and adding the contributions from all strips and dividing the term by the total surface area. The plots are given in Fig. 21. The error introduced for the Alboran is considerable because the density of the isobaric contours was too coarse, but the main features are visible in both plots.

3.7. WIND DATA

Wind data obtained from three land stations situated near the Alboran Sea are displayed in Fig. 22. The data are the daily midday observations published in the weather maps of the European Meteorological Bulletin (referenced in pressure section above).

4. Results

4.1. FLOATS

The computed float trajectories (and depths) are given in Fig. 23. Between the depths 220 m and 1100 m all of the floats were entrained in a broad cyclonic circulation pattern. The motion was slow, with stagnant periods interspersed with increased movement at an average speed of approximately 2.5 cm/s. Along the southern boundary, floats 1 and 2 moved westwords towards Gibraltar after reaching the Moroccan continental slope. Between days 112 and 119, float 2 moved with an average speed of about 5 cm/s. Floats 5 and 8 remained near the boundary at 35.6°N, 4.0°W for many days; and float 9, and finally also float 8, moved along the southern sloping bottom in the opposite direction, towards Alboran Island. Float 9 was in an acoustic shadow from day 75 to day 110 and was audible only from mooring B. Being located deep (1100 m), it moved in the channel, passed the Alboran Island, and returned along the northern slope of the channel. Float 4, moving in the northern part, was retrieved–and it is not clear if it would have moved to Gibraltar or turned south. Float 6 at day 92 had a power-loss in transmitted signal, and was later retrieved from near bottom (water had penetrated into the releaser). Figure 24 shows the time series of synchronized, decimated versions of filtered velocity data sampled every 12 h, and Fig. 25 shows the velocity components. Variability in amplitude and phase is large, with an average velocity amplitude in the range 2.4 to 3.7 cm/s.

4.2. CURRENT METERS

Figure 26 shows the time series of velocity vectors for all moored current meters. These are the synchronized and decimated versions of filtered data. The sampling interval was 12 h. The upper time series for each mooring is data from the shallow current meter; the lower one is for the deep current meter. The high correlation between the two series is clearly visible. The deep current meters at moorings A and B have increased amplitude compared to the others, probably caused by the currents along the Moroccan continental slope. Float velocities at these positions also indicated a quickening of the currents as compared with other positions (Fig. 25). Considerable variation in current amplitude and direction was recorded at site B. At site C, at the middle of the Alboran, very small currents were recorded. Figure 27 shows the time series of 12 hourly velocity components for all current meters. Plots (Fig. 28) of progressive vector diagrams for the upper and lower current meters emphasize the directional variability. Currents at site G show persistent western direction, currents at site F and upper site A change from south-east to north-west,

while currents at site B vary considerably at all times. Amplitude information from the upper current meters at sites B and F is not available because of current meter failure, on day 71 and day 46 respectively; in each case from the day of failure only the current direction was recorded at these sites.

4.3. CURRENT-METER FLOATS

Figures 29 and 30 show both the time variability and the space variability of the current flow recorded both by current meters and by floats. Figure 29 shows the current vector field in the Alboran every second day. This figure was created from filtered and decimated (to 12 h) data taken from Figs. 24 and 26. The data taken every two days neverthless displayed large variations in speed and direction of current. Figure 30 represents six time-windows (400 h each) in which the current meter data are represented as progressive vector diagrams and the float data are represented as the tracks during the same period. Except for the floats near the Moroccan continental slope, all floats persistently show the cyclonic nature of the circulation; however, the current meter data show the complicated changes in current speed and direction.

4.4. SURFACE LAYER

No current meter or float measurements were made in upper layer from the surface to 220 m. Only the satellite infrared images and CTD data can be used to interpret the surface layer motion.

Satellite data (IR images) show that there was considerable variation in the structure of the sea-surface temperature during the period of the experiment. They indicate the presence of an anticyclonic gyre in the south western part of the Alboran Sea. Figure 31 shows a few examples of the IR satellite data taken during the experiments. The darker shades in the images represent warmer water; however, the temperature variation for this period was only about 1 °C (12.8 to 13.7 °C). The images indicate considerable variations in the extension of the gyre, which is large in January and smaller and fragmented in February and March.

CTD measurements were performed in three periods as shown in Table 2. Figure 32 presents contours of the dynamic height anomaly at 100 m and 150 m relative to 200 m for January and April; the contours show anticyclonic circulation in the surface layer. (The data sets, however, are small). Figure 33 also shows anticyclonic circulation of the geostrophic current computed from the CTD cross-section on 8th March. The January and March CTD measurements reveal the well-developed gyre shown by sea-surface temperature data (Fig. 31); however the March data indicate a stronger anticyclonic circulation of smaller extent than the earlier data.

TABLE 2
CTD (N. Brown) casts, 1982

Cruise	Time (Julian Day)	Cast number(s)
I	22	1–3
	23	4–5
	24	6–9
	25	10–14
	26	15–16
	27	17–18
	28	19
	29	25–26
	30	27
	31	31
	32	32–34
	33	35–37
II	67	1–9
	68	10–14
	69	15–17
	70	18
III	115	1–2
	119	3–13
	120	14–23
	121	24–26

4.5. DEEP CTD CROSS-SECTION

Figures 34 to 37 present several cross-sections of salinity and potential temperature. All show the upward bending of deep isolines across the Moroccan continental slope. This bending represents the upwelling of the Deep Western Mediterannean Water. The effect is more pronounced in the western part of the Moroccan continental slope. The Levantine water-mass is concentrated in the middle of the Alboran. No upward bending of isolines that would indicate upwelling is detectable in the north of the Alboran. The intermediate maximum values of temperature and salinity which indicate Levantine water were lowered in the southern Alboran because the Levantine water was mixed with the Deep Western Mediterannean Water. The cross-section in Fig. 34 shows an example (day 67) of very strong upwelling near the southern boundary. To reveal this event in more detail plots of potential temperature versus salinity (θ/S plots) for the same cross-section are displayed in Fig. 38. This figure shows the absence of Levantine water maxima near the Moroccan continental slope and its presence in considerably shallower strata (250 m) in the middle

of the cross-section. Potential density cross-section corresponding to this energetic mixing is shown in Fig. 39, revealing that the density is a monotonic depth function, i.e. salinity and temperature effects are well balanced. The cross-section in Fig. 35 and the corresponding θ/S plots for some of its stations in Fig. 40a (from April 1982) do not show the energetic mixing even althouth it is only 23 km southeast of the location of energetic mixing described above. Likewise the more eastern cross-sections in Fig. 36 (with corresponding θ/S plots in Fig. 40b) and Fig. 37 show the upward bending of isolines, but of smaller extent and intensity.

4.6. DEEP AND UPPER LAYER CORRELATION

The set of SST satellite images taken from day 61 to day 69 in 1982 are given in Fig. 41. They show the growth of a new energetic anticyclonic gyre near Ceuta. It reached its maximum at day 67; later the area was covered by clouds but there is an indication that on day 69 it apparently merged with the large anticyclonic gyre to the east. To establish the depth of this anticyclonic gyre the simultaneous data from current meters moored in its area and CTD casts were examined. The CTD cross-section taken on day 67, and displayed in Fig. 34, shows very active dynamics and an eddy-like structure extending to 800 m. Geostrophic calculations of current based on this cross-section revealed a very energetic anticyclonic geostrophic current for the upper layer, reaching 80 cm/s as shown in Fig. 33. Calculation of deep geostrophic current based on the same cross-section showed the continuation of anticyclonic circulation from the surface to 800 m when the level of no-motion was chosen at 800 m (see Fig. 42a) and cyclonic motion when the level of no-motion was chosen at 200 m (Fig. 42b). Current-meter data at mooring A for the same period (day 60 to day 70) showed variable current, indicating that no eddy reached the instrument. Current-meter data at mooring F were in agreement with the assumption of a deep-reaching anticyclonic gyre.

Another attempt to correlate data of the deep layer with the upper layer circulation is shown in Fig. 43, in which SST satellite images cover days 22, 29, 30, 31, and 32, and the CTD data cover the period from the day 22 to day 33. Contours of the dynamic height anomaly in Fig. 32, which were computed from this set of CTD data, show the large-scale anticyclonic circulation in agreement with the satellite data from day 22. Two cross-sections of geostrophic current in Fig. 44 were computed from casts 11 to 14 taken at day 25 (Fig. 44a) and casts 10 to 16 taken between days 25 and 26 (Fig. 44b). The level of no-motion was chosen in agreement with the float motions, at 220 m. The upper layer in Fig. 42b shows the broad anticyclonic circulation between casts 19 to 15. The same feature appears in Fig. 42a. Deep geostrophic currents show cyclonic motion with a direction which is in agreement with data for the appropriate period (Fig. 29) from current meters at moorings F and A.

Two cross-sections of geostrophic currrent computed from the April 1982 CTD data

are shown in Fig. 45. This result indicates that the surface anticyclonic gyre was small, and was located only in the south-western corner of the Alboran. The cross-section A shows current directed to the east in the upper layer across the whole cross-section, and possibly cyclonic motion in the deeper layer. Cross-section B indicates the return current as being in agreement with the data of the current meters at mooring A (shown in Fig. 29 for day 114). A schematic of the deep currents is included in the same figure. The level of no-motion for the geostrophic calculation was assumed to be 220 m.

4.7. METEOROLOGICAL FORCING

4.7.1. Correlation with deep currents. Two time series of averaged atmospheric pressure, called ALBORAN and WESTMED as mentioned earlier at Sect. 2.6 were cross-correlated with current-meter data to establish the effect of pressure on currents in the Alboran. To examine the spectral content of the averaged atmospheric pressure series, autospectra were computed for both series. They are displayed in Fig. 46 with spectral peaks for the Alboran at periods of 9, 7, 4, 2.2, and 1.3 days; and for WESTMED at periods of 9, 7, 4, 3.3, and 2.2 days. The time series are too short (for periods > 100 h) to establish the low frequency spectral content with confidence, which is why autocorrelations were computed. These are shown in Fig. 47, indicating the presence of lower frequency periodicities with durations of 17, 12, and 9 days for WESTMED series and 13 and 9 days for ALBORAN series.

To examine the cross-correlation between atmospheric pressure and current-meter data, correlations were computed for each current-meter component and pressure and current speed and pressure. The results are presented in Fig. 48 for the ALBORAN and in Fig. 49 for the WESTMED. Time delay in the figures is the delay of current relative to pressure (minus signifies pressure in advance). The numbers in the lefthand corner of each small figure relate to the highest correlation and its time delay.

The cross-correlations are sometimes as high as 0.6, but the delays are so large that they lose physical meaning. In addition there is no cross-correlation extreme at the same delay time for all of the current meters, which is what is expected in the case of barotropic response. The resulting cross-correlations between current and ALBORAN pressure do not differ from those between current and WESTMED pressure.

Figures 50 and 51 present cross-correlations between float data and atmospheric pressure. Four floats with the longest deployment time were chosen. Figure 50 shows the cross-correlations between the pressure and velocity amplitudes of the floats; in Fig. 51 velocity is replaced by variation in variable position. The variation-in-position variable was created from velocity data by subtracting the corresponding average velocity component and integrating the obtained variable over time. The

results are similar to the results of the cross-correlations between the pressure and current-meter data described above.

4.7.2. Correlation between atmospheric conditions and the position and extension of surface anticyclonic gyre. To correlate the atmospheric variables, namely wind and atmospheric pressure, with the position and extension of the anticyclonic gyre located in southwestern Alboran Sea, and likewise to correlate the wind and atmospheric data with the changes in position and changes in extension of this anticyclonic gyre, satellite infrared images and wind and pressure data from Fig. 22 were used. The atmospheric pressure data in this figure are marked only qualitatively (as high or low) and indicate an average WESTMED pressure for the particular periods shown in this figure.

Observations for the period from January 22 to February 1 are summarized as follows:

The satellite IR images in Fig. 43 and the data in Fig. 22 reveal the large gyre on January 22 when the average pressure for WestMed was high (1020 mbar) and a westerly wind with an amplitude of less than 10 n.mi was blowing.

Lower pressure (1015 mbar) between January 24 to 29 and stronger (> 20 n.mi) north-westerly wind probably pushed the gyre to the east and flattened it (day 29), which is in agreement with a Cheney and Doblar (1978) hypothesis.

High pressure (1025 mbar) started on day 29 and continued (until day 44) with an easterly wind blowing for two days. This could be the reason for the observation of an enlarged and compact gyre on day 31, which is also in agreement with the Cheney and Doblar hypothesis.

The change in wind direction to westerly between days 30 and 31, and continuing high pressure on day 32, correspond to the satellite image for this day, which shows strong partition of the gyre. However there are not enough CTD casts to document the partitioning and it is possible that, as described by Bucca and Kinder (1984), it does not extend very deep.

The CTD data cover a period of 10 days (days 22 to 32) and contours of the dynamic height anomaly derived from this data at depths of 100 m and 150 m (with a reference level of 200 m) show the large anticyclonic gyre shifted slightly to the east (Fig. 32), indicating that the IR image structure does not extend deeper than 100 m.

The next observation relates to day 49: the IR image (Fig. 31) and the atmospheric data (Fig. 22) show a situation described by Cheney and Doblar (1978), where low average WESTMED pressure (1012 mbar) and westerly winds shifted the gyre to the east, away from its average position.

Another observation worth discussion is taken from the period between

day 61 and day 69. The satellite images are given in Fig. 41. The atmospheric conditions (Fig. 22) were high (1020 mbar) WESTMED pressure, starting on day 60, and wind changing from westerly (day 59) to south or north easterly (day 61 and later) with very strong amplitudes (20 n.mi) at stations 1 and 3 respectively for the period from day 63 to day 65. The satellite images show a new gyre is growing under this condition, near to Ceuta as described above in the section about satellite images. Under high pressure and generally easterly winds the gyre should be stable, as assumed by Cheney and Doblar (1978), in contradiction to the above observation.

In addition to the difficulties of explaining the migration and extension of the gyre, there are difficulties in explaining the satellite observation of the creation and growth of new vortexes near Ceuta. Possibly the wind amplitude and even relatively small directional variations are the important factors in the creation and growth of a new gyre.

4.8. SPECTRA OF CURRENT-METER AND FLOAT DATA

Autospectra for each current-meter component and rotational spectra for all 12 current meters are presented in Fig. 52; the 90% confidence limit of the Gaussian distribution is indicated. These are high-frequency spectra and are produced from the original data. Tidal variations, mainly the semidiurnal tide and inertial oscillations are clearly identifiable. In many current meters there is a peak which has a period of 6 h, indicating the tidal nonlinearity. The deeper (412 m) current meter at mooring G gave a pronounced peak with a period of around 1.5 h; no such peak was present at the same time at the depth of 230 m. The current meters at E and the shallow (300 m) current meter at F show the presence of the 1.5 h signal. The deep (400 m) current meters at G and at A (793 m) display the spectral peak as a period of 40 min, which indicates the presence of solitons. Low-frequency current-meter spectra (auto and rotary) are presented in Fig. 53 and float spectra are presented in Fig. 54; they were obtained by averaging the spectra of all of the current meters and floats, respectively. It is interesting to compare the spectral peaks with those of the average atmospheric pressure (Figs. 46, 47) and with 1980 current-meter data (Pistek, 1984). Spectral peaks with durations of 4, 7 and 9 days are visible in the atmospheric pressure spectra and were also present in the 1980 current-meter data; they are also visible in the current-meter spectra (4 and 7 days) in Fig. 53 and the float spectra (9 days) in Fig. 54. Longer periods are detectable in the atmospheric pressure data (Fig. 47): 13–14 days for the ALBORAN and 12 and 17 days for the WESTMED. These periods are visible in the current-meter spectra (12 and 17 days) in Fig. 53 and the float spectra (13.5 days) in Fig. 54. The 1980 current-meter spectra also had a peak of 14 days.

4.9. NONLINEAR INTERNAL WAVES

Current-meter data from the current meters with the short sampling interval (4 min) show the presence of nonlinear internal waves. These waves are created by the semidiurnal tide near the sill of the Strait of Gibraltar. They propagate to the east (Frassetto, 1964; Ziegenbein, 1969)), and the eastern end of the Strait of Gibraltar acts like a slit to them. When they propagate into the Alboran it is in all directions, and the variable depth and strong current cause assymetrical propagation. It has been assumed that they propagate only in the middle and northern part of the Alboran, but our measurements show their presence also in the southern part. For example, two current meters positioned in the southern part of the Alboran at moorings A and B (Fig. 5) and depths of 793 m and 763 m respectively registered a high frequency signal with a period of 20 to 40 min. Neap- and spring-tide variability in the signal amplitude is clearly visible in the data. Examples of the signal (possibly solitons) are presented in Figs. 55 and 56.

Figure 55 shows the east-west and north-south velocity components from current-meter data at mooring A. The legend N-S FILT denotes the high-pass-filtered, north-south velocity component of the same data. The filtered data show that there is almost constant 'ringing', indicating an almost continuous presence of nonlinear internal waves.

Figure 56 shows the two velocity components for the same time window at mooring B. The spectra for moorings A and B are given in Fig. 57, with numbers near the peaks indicating the wave periods in minutes. The sharp cut-off at 100 min is due to filtering.

5. Discussion and conclusions

Between depths of 220 m and 110 m, weak coherent cyclonic motion with a vortex centre at about 35.75°N, 4.25°W persisted in the Alboran Sea during the 3-month period of measurement. Both float and current-meter data are in agreement on this. Vortex circulation varied, with periods of stagnation being followed by faster motion averaging between 2.4 and 3.7 cm/s. Current-meter data show that the spatial extent of this vortex varied with time, sometimes encompassing a large part of the central and western Alboran and at other times it was shrinking. The Moroccan continental slope marked the southern boundary of this circulation. Upwelling currents on that boundary are much smaller than the motion parallel to the topography. When the floats reached this boundary west of 4.0°W (floats 1 and 2) they moved towards Gibraltar, with an average speed, for float 2 (between days 112 and 119), of about 5 cm/s. This is in agreement with previous data (Bryden and Stommel, 1982, and Pistek, 1984).

Current-meter data from moorings F and A sometimes showed currents towards Gibraltar. The lack of constancy reflects the variability in the extension of the cyclonic vortex. Floats reaching the boundary east of 4.0°W moved in the direction of Alboran Island, but not persistently, which is also in agreement with the current-meter data at mooring B. In agreement with Pistek (1984), flow in the central Alboran was slow. Floats deployed in the middle section of the Alboran moved cyclonically and did not cross into the area west of 4.5°W, indicating the main path of Levantine and Deep Western Mediterranean waters. Float 9, deployed at a depth of 1100 m, indicated that the flow of the Deep Western Mediterranean water into the Alboran is along the northern slope of the deep Alboran channel. Also the current-meter data from mooring G (depths of 228 m and 412 m) indicated persistent flow from the east. Kinder's (1984) data from current meters positioned in the western Alboran north of 36°N showed the flow at 500 m to the west; also floats 4 and 6 deployed near the Spanish continental slope showed that there is a partial flow of Levantine and Deep Western Mediterranean waters along the Spanish continental slope towards Gibraltar. However there was no indication in the north-western Alboran, either from CTDs or float motions, of the steady flow displayed along the western Moroccan continental slope. Float 4, for instance, deployed for 32 days at a depth of 470 m, stagnated in the north-western Alboran for more than 10 days. Current-meter data from mooring E (depths of 385 m and 638 m) also showed a small and variable current for more than one-third of the deployment time, instead of a steady westward flow.

The potential temperature and salinity structures in the Alboran Sea exhibit very sharp slopes in the isotherms colder than 12.9 °C and in the isohalines below the salinity maximum at the Moroccan continental slope. This feature was first observed

by Bryden and Stommel (1982) and later confirmed by many other investigators. This structure is an indicator of the mixing of Levantine and Deep Western Mediterranean waters and, in connection with the enhanced flow along the slope towards Gibraltar as described above, indicates the path of unmixed flow of the portion of Deep Western Mediterranean water out of the Mediterranean to the Atlantic. The bending of isolines (March, April data) was more pronounced in the western than in the central Alboran, and more vigorous in March than in April. The corresponding isopycnals (potential sigma) exhibit a similar slope, indicating that once established it would not be difficult for Deep Western Mediterranean water to move upwards along them and eventually out of the Alboran to the Atlantic.

The cause of this feature is not understood. Alboran circulation is in general part of Mediterranean thermohaline circulation. It is known that the Levantine and Deep Western Mediterranean waters ascend as they move westward from the eastern Alboran. Stommel, Bryden and Malgelsdorf (1973) discussed the importance of Bernoulli's effect for this upwelling, and later Bryden and Stommel (1982) discussed the interplay of vorticity and Bernoulli's upwelling in the enhancing of the anticyclonic circulation. The deep extension of the anticyclonic gyre and its interaction with the Moroccan continental slope were assumed by these authors to be a source of forcing for enhanced current and upwelling. In the same reference the authors also discuss the effect that the sucking created by the outflow of water across the sill in the Strait of Gibraltar (phenomenon well-known in relation to fresh-water dams) has on upwelling of the Deep Western Mediterranean water.

The preliminary results of computer modelling done by Preller (personal communication) show very slow cyclonic deep layer motion forced by bottom topography. Possibly this effect in combination with the others, mentioned above, determine the deep circulation in the Alboran Sea.

To find out the depth and the lateral extension of the surface circulation, some satellite and CTD observations were made during the experiment in order to indicate the upper-layer structure. Satellite infrared images taken during the experiment show the existence of the upper-layer anticyclonic gyre in the south-western Alboran Sea. February and March images and March CTD data show the smaller gyre with its eastern boundary around 4.5°W. Likewise, April CTD data show a smaller extent of anticyclonic circulation. Calculations of geostrophic current for the cross-sections of CTDs are in agreement with the current-meter and float data if the no-motion level is set at 200 m, as they show anticyclonic motion in the upper layer with cyclonic motion beneath it. Specific attention was devoted to the 'march eddy'; which is an anticyclonic eddy developed near Ceuta. Infrared satellite images followed its growth from day 61 to 67. A CTD cross-section was made on day 67 and showed strong bending of isolines and an anticyclonic geostrophic current of 80 cm/s in the upper layer. But its strength diminished rapidly with depth. Neverthless, it might reach to the bottom over the Moroccan borderland

(400 m depth) and enhance the upwelling across the Moroccan continental slope as indicated by Bryden and Stommel (1982).

In addition to circulation studies a qualitative evaluation was made of the influence of atmospheric pressure on deep circulation and the interdependence of pressure, wind and changes in the surface anticyclonic gyre as indicated by infrared satellite images.

Studies of cross-correlations were made between the atmospheric pressure averaged over the whole Western Mediterranean Sea and over the Alboran Sea. The current-meter or float data did not show any pronounced dependence, even although many spectral peaks of the same frequency were found in both data sets. In agreement with earlier works, the low average Western Mediterranean atmospheric pressure and westerly winds are associated with the shift of the anticyclonic gyre to the east while the opposite conditions stabilize and enlarge the gyre in the western Alboran Sea. When the anticyclonic gyre shifts to the east, a new but smaller anticyclonic gyre often develops to the west of it. Our observations for March 82 show that a new energetic anticyclonic gyre also developed under the opposite conditions, indicating that some other variables are important in the change of vorticity field.

Finally two current-meter measurements positioned in the southern Alboran Sea, near the Moroccan continental slope at depths of 793 m and 763 m, yielded a signal related to the nonlinear internal waves. These waves were generated near the sill of the Strait of Gibraltar and propagated to the east. They had not been detected previously in the southern Alboran, and it was assumed that they propagate only in the northern part. Our data show that there is propagation symmetry.

Spectral analysis of the float and current-meter data showed strong semi-diurnal tidal variation and inertial oscillations. The peak corresponding to a 6 h periodicity indicates the nonlinearity of the semi-diurnal tide. The 1.5 h peak that is clearly visible at 412 m in the deep Alboran channel has not been explained. Most of the long-period variations visible in the averaged float and current-meter spectra are also visible in the atmospheric variations.

The most important engineering aspect of this experiment was the investigation of the feasibility of using autonomous listening stations for unattended acoustic-tracking of mid-range Swallow-type floats. The results show that it is indeed feasible, even for a variable bathymetric environment like the Alboran Sea.

References

ALLAIN, C. L'Hydrologie et les courants du Détroit de Gibraltar pendant l'été de 1959. *Revue des Travaux, Institut des Pêches Maritimes*, **28**, 1964: 1-99.

BETHOUX, J.P. Budgets of the Mediterranean Sea. Their dependance on the local climate and on the characteristics of the Atlantic waters. *Oceanologica Acta*, **2**, 1979: 157-163.

BETHOUX, J.P. Mean water fluxes across sections in the Mediterranean Sea, evaluated on the basis of water and salt budgets and of observed salinities, *Oceanologica Acta*, **3**, 1980: 79-88.

BRADLY, A. and TILLIER, P. Mesoscale Lagrangian measurement system. ICES Hydrographic Committee, Proceedings CM 1980/C7. Copenhagen, Comité International pour l'Exploration de la Mer/International Committee for the Exploration of the Seas, 1980.

BRYDEN, H.L., MILLARD, R.C. and PORTER, D.L. Technical Report: CTD observations in the western mediterranean Sea during cruise 118, LEG 2 of R/V CHAIN, Feb. 1975. WHOI-78-26, Woods Hole Oceanographic Institution, Woods Hole, Massachusetts 02543, March 1978.

BRYDEN, H.L. and STOMMEL, H.M. Origin of the Mediterranean outflow. *Journal of Marine Research*, **40** (supplement), 1982: 55-71.

BUCCA, P.J. and KINDER, T.H. An example of meteorological effects on the Alboran Sea gyre. *Journal of Geophysical Research*, **89**, 1984: 751-757.

CHENEY, R.E. and DOBLAR, R.A. Structure and variability of the Alboran Sea frontal system. *Journal of Geophysical Research*, **83**, 1978: 4593-4597.

CREPON, M. Influence de la pression atmosphérique sur le niveau moyen de la Méditerranée occidentale et sur le flux à travers le Détroit de Gibraltar. *Cahiers Océanographiques*, **7**, 1965: 15-32.

DEACON, M. Scientists and the Sea, 1650-1900: A Study of Marine Science. New York, NY, Academic Press, 1971: p. 445.

DEFANT, A. Physical Oceanography, Vol. 1, New York, NY, Pergamon Press, 1961: 729.

FRASSETTO, R. Short-period vertical displacements of the upper layers in the Strait of Gibraltar, SACLANTCEN TR-30, Parts 1 and 2. La Spezia, Italy, SACLANT ASW Research Centre. [AD 808 764/AD 808 765].

GALLAGHER, J.J., FECHER, M. and GORMAN, J. Project HUELVA, Oceanographic/acoustic investigation of the western Alboran Sea, NUSC 6023. New London CT, Naval Underwater Systems Center, 1981.

GARRETT, C. Variable sea level and strait flows in the Mediterranean: a theoretical study of the response to meteorological forcing. *Oceanological Acta*, 1983: 79-87.

GROVES, G.W. Numerical filters for discriminating against tidal periodicities. *Trans. American Geophysical Union*, **36**, 1955: 1073-1084.

KINDER, T.H. Current meter measurements in the northwestern Alboran Sea. *In*: PARRILLA, G. *ed.* Preliminary Results of the Donde Va meeting in Fuengirola, Malaga, Spain,

18-21 October 1983, Informes Tecnicos Instituto Español de Oceanografia 24 1984. Madrid, Spain. Inst. Espanol de Oceanografia. Alcala, **27**, 1984: 159-167.

LACOMBE, H. Contribution à l'étude du régime du détroit de Gibraltar. 1. Etude dynamique, *Cahiers Océanographiques*, **13**, 1961: 73-107.

LACOMBE, H. Le Détroit de Gibraltar, Océanographique physique. *Notes et Mémoires du Service Géologiques du Maroc*, **22**, 1971: 111-146.

LACOMBE, H. and RICHEZ, C. Contribution à l'étude du régime du détroit de Gibraltar. 2. Etude hydrologique, *Cahiers Océanographiques*, **13**, 1961: 276-291.

LACOMBE, H., TCHERNIA, P., RICHEZ, C. and GAMBERONI, L. Deuxième contribution à l'étude du régime du détroit de Gibraltar (Travaux de 1960), *Cahiers Océanographiques*, **6**, 1964: 283-314.

LANOIX, F. Project Alboran: étude hydrologique et dynamique de la Mer d'Alboran d'après les travaux effectués dans le cadre du Projet Alboran (juillet et août 1962), Rapport Technique OTAN no. 66. Bruxelles, Belgique, Organisation du Traité de l'Atlantique Nord, Sous-Comité Océanographique, 1974.

LA VIOLETTE, E.P. The advection of submesoscale thermal features in the Alboran Sea gyre. NORDA Technical Note 240. Mississippi, MS, Naval Ocean Research and Development Activity, NSTL, 1983.

MEDOC Group. Observation of formation of deep water in the Mediterranean Sea. *Nature*, **227**, 1970: 1037-1040.

OVCHINNIKOV, I.M., KRIVOSHEYA, V.G. and MASKALENKO, L.V. Anomalous features of the water circulation of the Alboran Sea during the summer of 1962. *Oceanology*, **15**, 1976: 31-35.

OZTURGUT, E. The sources and spreading of the Levantine intermediate water in the eastern Mediterranean, SACLANTCEN SM-92. La Spezia, Italy, SACLANT ASW Research Centre, 1976. [AD B 018 619].

PARRILLA, G. *ed.* Preliminary Results of the Donde Va meeting in Fuengirola, Malaga, Spain, 18-21 October 1983, Informes Tecnicos Instituto Español de Oceanografia 24 1984. Madrid, Spain. Inst. Espanol de Oceanografia. Alcala, **27**, 1984: 159-167.

PHILIPPE, M. and HARANG, L. Surface temperature fronts in the Mediterranean Sea from infrared satellite imagery. *In*: NIHOUL, J.C.J. *ed.* Hydrodynamics of Semi-Enclosed Seas. Amsterdam, Elsevier, 1982: 91-128.

PISTEK, P. Deep circulation in the Alboran Sea. *In*: NATO SACLANTCEN. Papers presented to the 42nd meeting of the SACLANTCEN Scientific Committee of National Representatives, 10-13 May 1983, SACLANTCEN CP-33, NATO CONFIDENTIAL, SACLANT ASW Research Centre, 1983: 5-1 to 5-16. [AD C 952 418].

PISTEK, P. Deep water mass circulation in the western Alboran basin: measurements in July and September 1980 (ALBORAN I experiment). SACLANTCEN SR-81, La Spezia, Italy SACLANT ASW Research Centre, 1984. [AD A148 566]

PISTEK, P.,de STROBEL, F. and MONTANARI, C. The use of SACLANTCEN - engineered floats for oceanographic research, NATO UNCLASSIFIED. *In*: NATO SACLANT

ASW Research Centre. Papers presented to the 37th Meeting of the SACLANTCEN Scientific Committee of National Representatives, 14-16 October 1980. SACLANTCEN CP-28, NATO CONFIDENTIAL, La Spezia, Italy, SACLANT ASW Research Centre, 1980: 8-1 to 8-5 [AD C 024 237].

PISTEK, P., de STROBEL, F. and MONTANARI, C. Low-frequency recoverable acoustic swallow floats for measuring mid and deep water circulation. Atti del 6° Congresso della Associazione Italiana di Oceanologia e Limnologia April 1984, Livorno, Italy.

PISTEK, P., de STROBEL, F. and MONTANARI, C. Deep Sea Circulation in the Alboran Sea. To be published in: *Journal of Geophysical Research*, 1985.

PORTER, D.L. The anticyclonic gyre of the Alboran Sea, independent research report from MIT-WHOI joint program. Woods Hole MA, Woods Hole Oceanographic Institution, 1976.

PRELLER, R. and HURLBURT, H. A reduced gravity numerical model of circulation in the Alboran Sea. *In:* NIHOUL, J.C.J. *ed.*, Hydrodynamics of Semi-Enclosed Seas. [ISBN 0-444-42077-0]. Amsterdam, Elsevier, 1982: pp. 75-90.

SANKEY, T. The formation of deep water in the northwestern Mediterranean. *Progress in Oceanography*, **6**, 1973: 159-179.

STOMMEL, H. Deep winter-time convection in the western Mediterranean Sea. *In*: Studies in Physical Oceanography, Vol. 2, A.L. Gordon,*ed.* Gordon and Breach, New York, 1972: 232.

STOMMEL, H.M., BRYDEN, H. and MALGELSDORF, P. Does the Mediterranean outflow come from great depth? *Pure and Applied Geophysics*, **105**, 1973: 879-889.

TILLIER, P. Expendable mid-range SOFAR floats and shipborne receiver. *Polymode News*, **73**, 1980: 7-8.

WANNAMAKER, B. The Alboran Sea Gyre: ship, satellite, and historical data, SACLANTCEN SR-30. La Spezia, Italy, SACLANT ASW Research Centre, 1979. [AD A 081 852]

WANNAMAKER, B. A system for receiving and analysing meteorological satellite data at small meteorological/oceanographic centres or aboard ship, SACLANTCEN SR-74, La Spezia, Italy, SACLANT ASW Research Centre, 1983. [AD A 137 215]

WHITEHEAD, J.A., Jr. and MILLER, A.R. Laboratory simulation of the gyre in the Alboran Sea. *Journal of Geophysical Research*, **84**, 1979: 3733-3742.

WUST, G. On the vertical circulation of the Mediterranean Sea. *Journal of Geophysical Research*, **66**, 1961: 3261-3271.

ZIEGENBEIN, J. Spatial observations of internal waves in the Strait of Gibraltar, SACLANTCEN TR-147. La Spezia, Italy, SACLANT ASW Research Centre, 1969. [AD 856 SACLANTCEN 028]

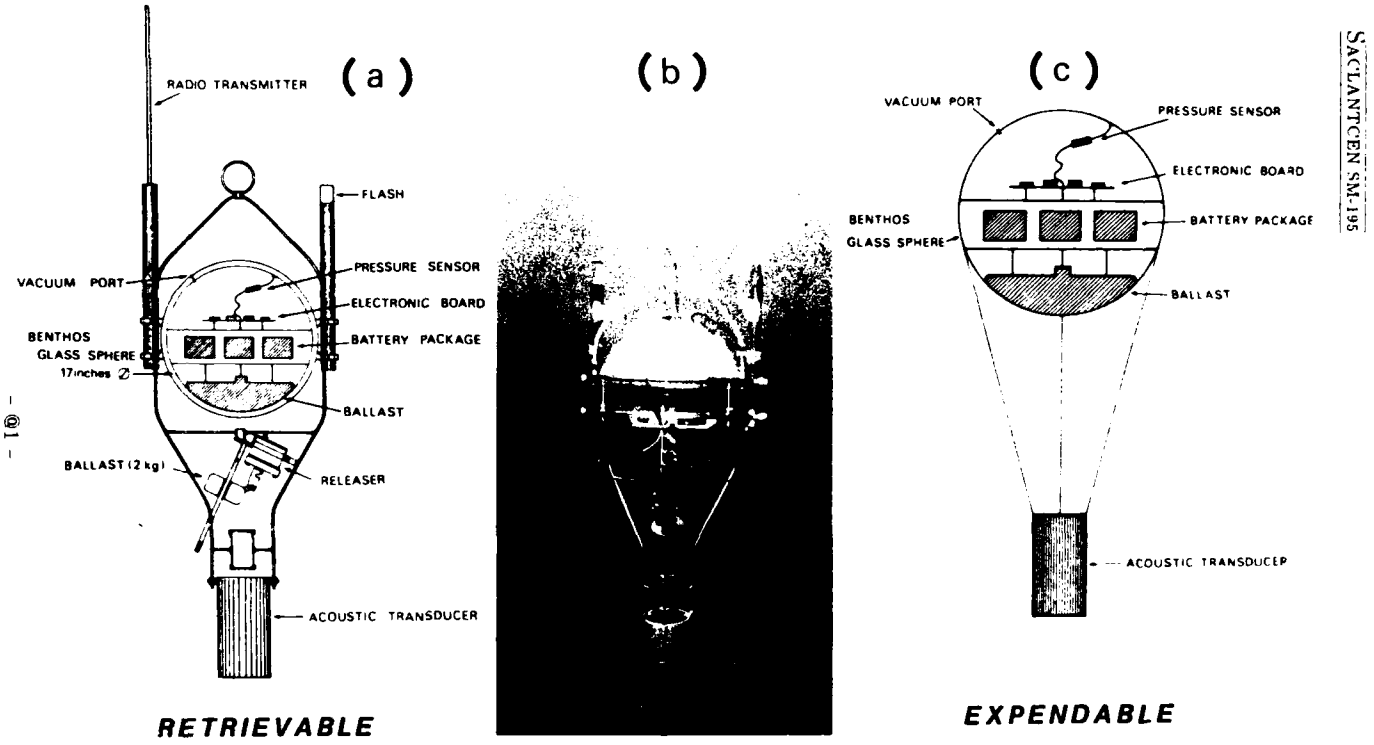

SACLANTCEN SM-195

Fig. 1. Deep drifting floats: (a) modified SACLANT type - retrievable; (b) photograph of SACLANT float after deployment; (c) benthos type - expendable

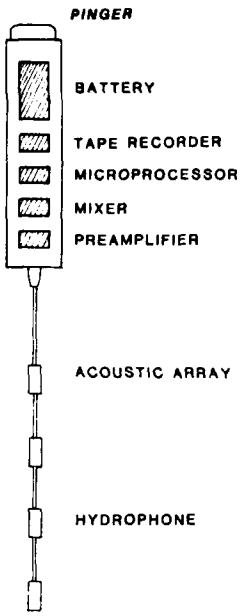

Fig. 2. Automatic listening station (ALS) housed in an aluminium tube which has the hydrophone array (4 hydrophones spaced at 95 m intervals and excluding signals from the vertical direction) hanging below it; the system is mounted in line with the mooring.

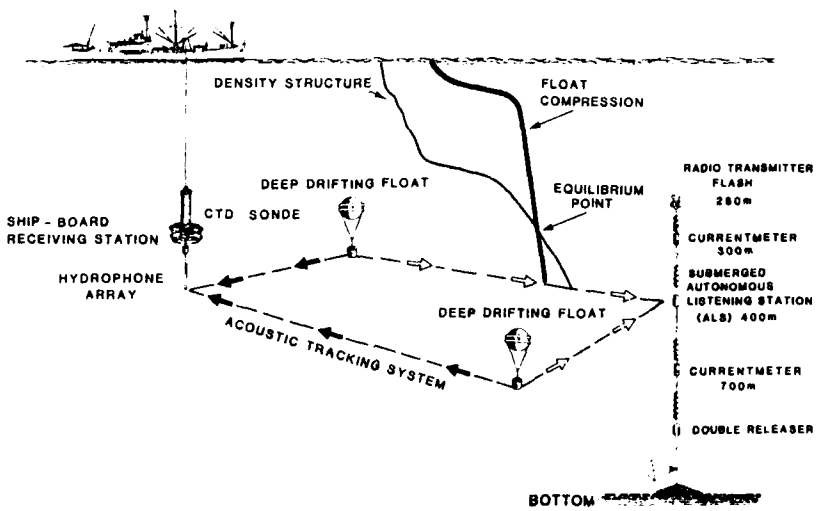

Fig. 3. Deployment of equipment and the tracking of floats. [The ALS and ship-board station track the floats; density structure and compression of floats establish the deployment depth (equilibrium point).]

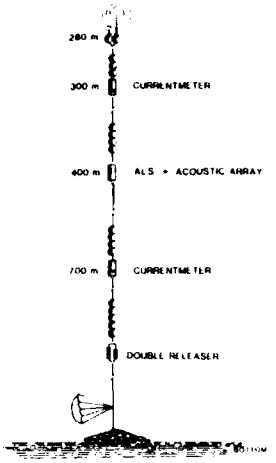

Fig. 4. Subsurface mooring: schematic diagram of current meter mooring. Six moorings of this type were deployed with two current meters on each. In addition to the two current meters, three of the moorings had an ALS. An EG&G transponder and a realeaser were near the bottom of each mooring. Buoyancy was distributed linearly along the mooring.]

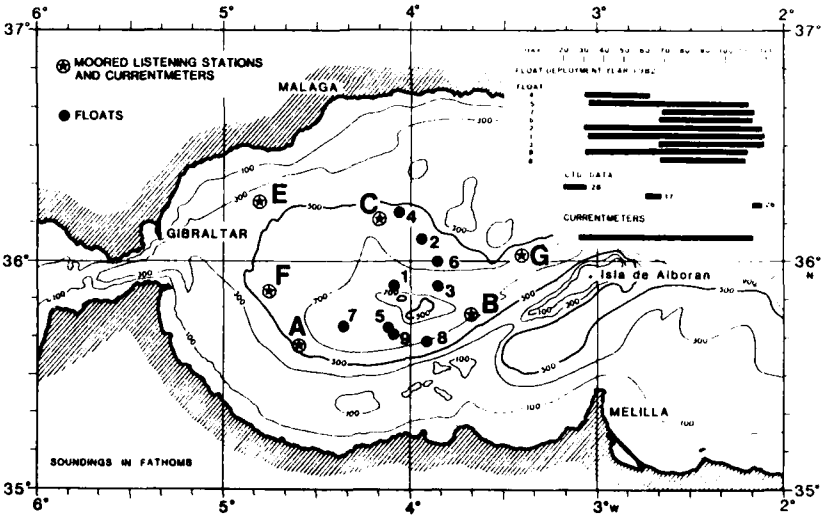

Fig. 5. Positions and deployment period for floats and current meters. [A, B, C, E, F, G mark the sites of mooring deployment, two current meters were deployed on each mooring. Three ALS were on moorings A, B, C at 400 m. Dots marked with numbers signify the deployment positions of individual floats (depths given in Fig. 23). Schematic diagram of the deployment period for floats, CTDs, and current meters is at the right corner.]

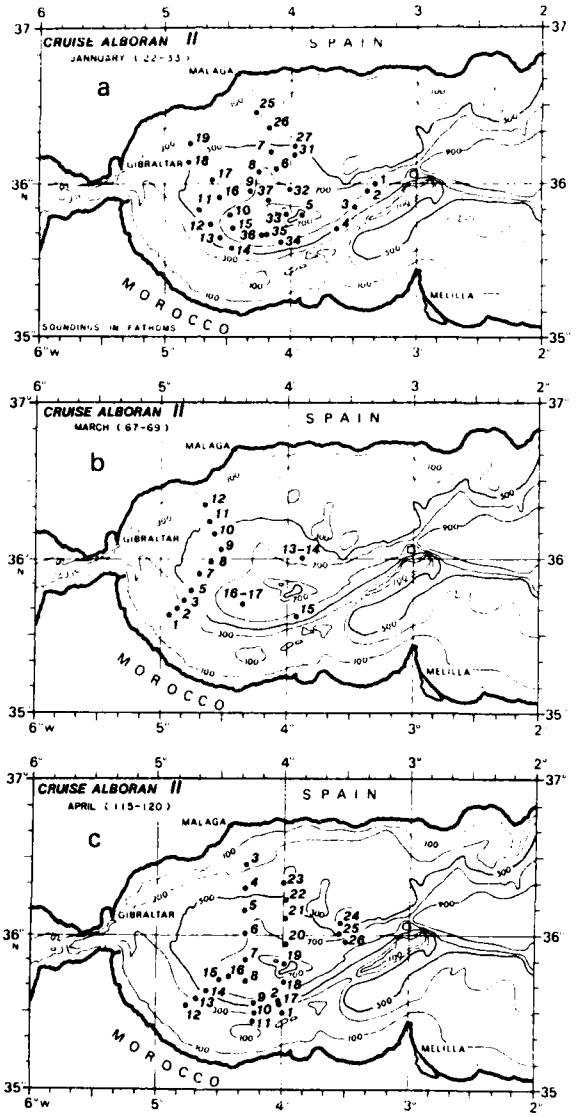

Fig. 6. Positions of CTD casts: (a) CTD casts during January 1982 (days 22 to 33); (b) CTD casts during March 1982 (days 67 to 70); (c) CTD casts during April 1982 (days 115 to 121).

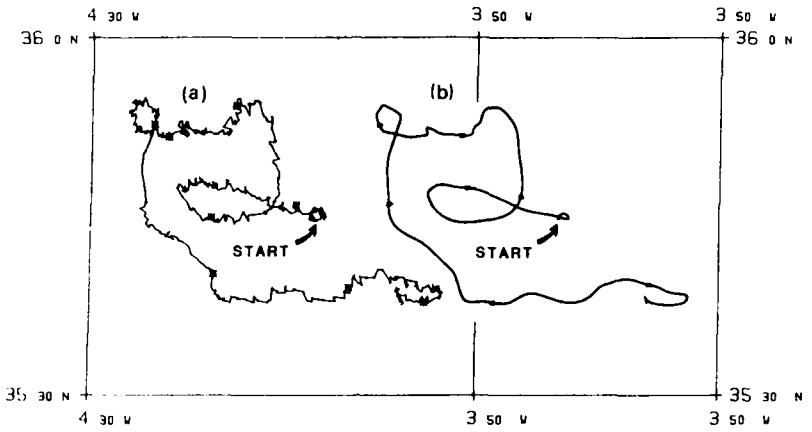

Fig. 7. Example of float track (float 5): (a) from raw 2-hourly data (tides and inertial oscillations are visible but not well resolved); (b) after filtration.

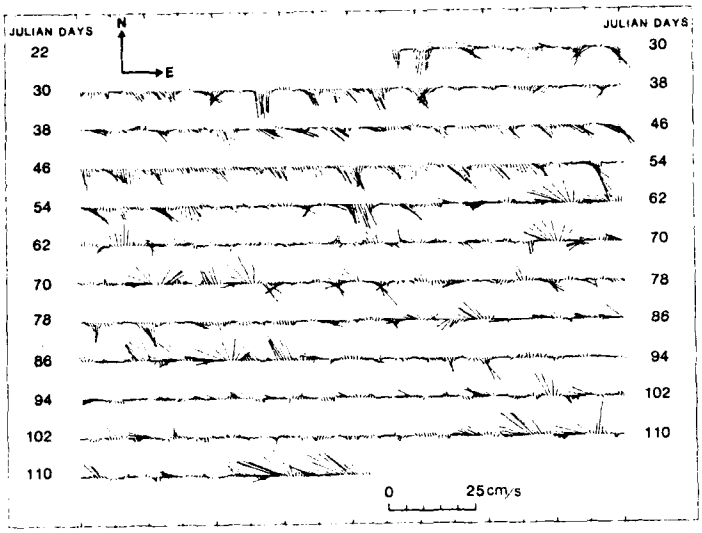

Fig. 8. Velocity vector time series of hourly NBA current meter data: Position A, depth 326 m; Jan, Apr 1982.

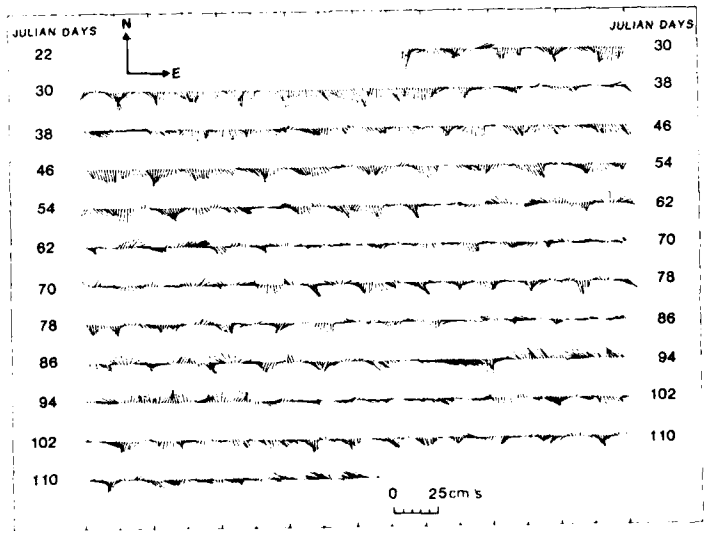

Fig. 9. Velocity vector time series of hourly NB acoustic current meter data: Position A, depth 793 m; Jan, Apr 1982.

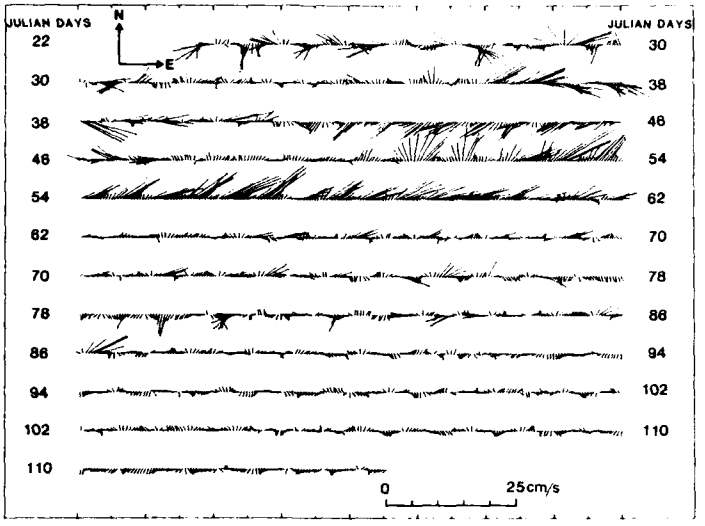

Fig. 10. Velocity vector time series of hourly NBA current meter data: Position B, depth 331 m; Jan, Apr 1982. [From day 62 amplitude is diminished because of malfunctioning and only the phase information is valid. The current direction correlates well with the deep current meter (at 763 m) on the same mooring (Fig. 11).]

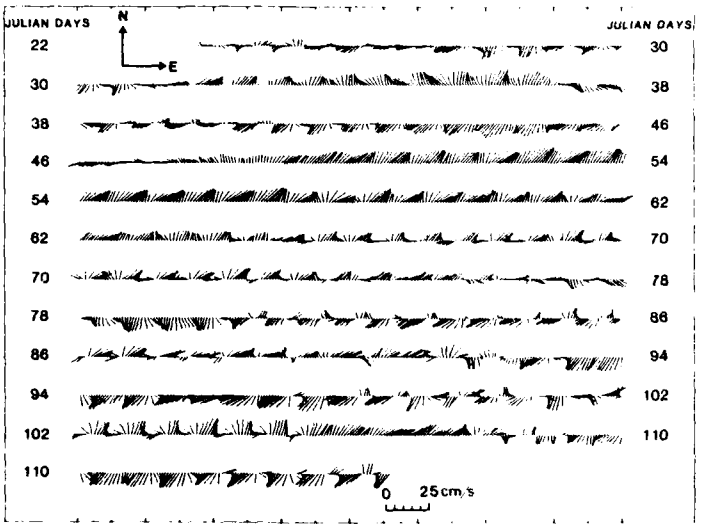

Fig. 11. Velocity vector time series of hourly Niel Brown acoustic current meter data: Position B, depth 763 m; Jan, Apr 1982.

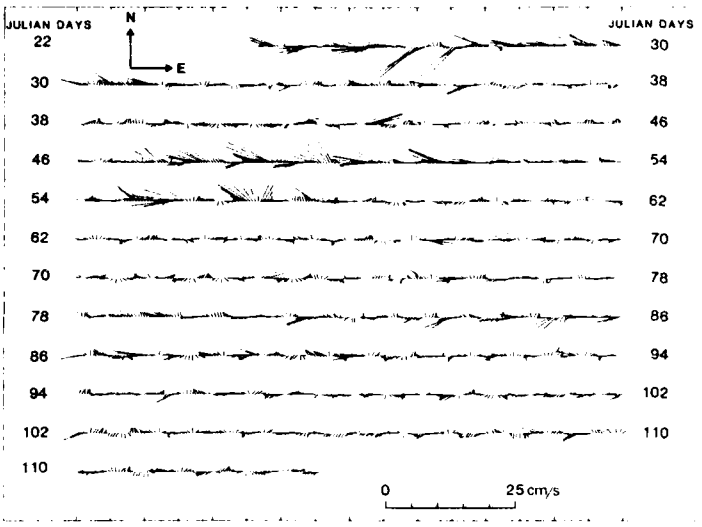

Fig. 12. Velocity vector time series of hourly NBA current meter data: Position C, depth 350 m; Jan, Apr 1982.

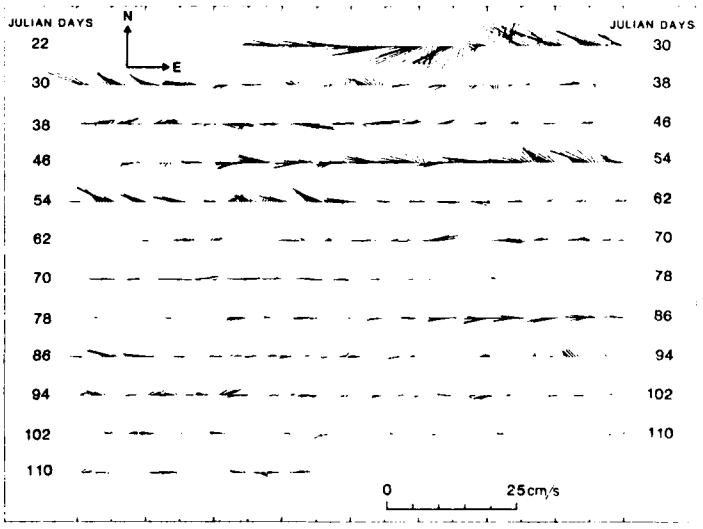

Fig. 13. Velocity vector time series of hourly Weller current meter data: Position C, depth 725 m; Jan, Apr 1982.

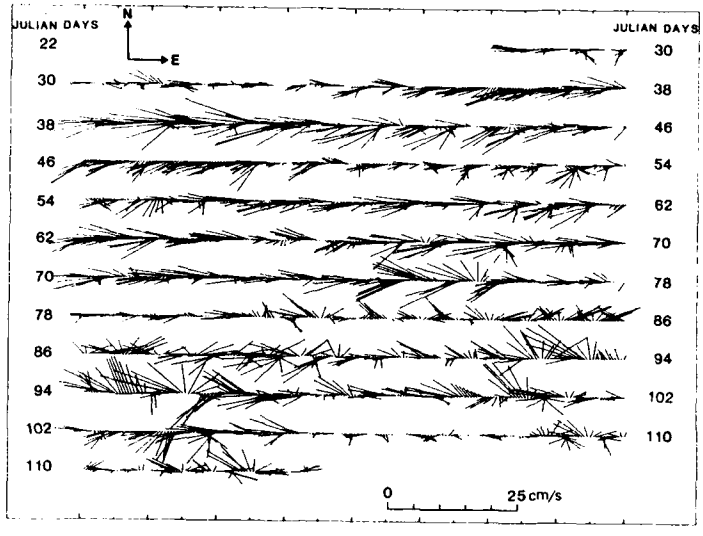

Fig. 14. Velocity vector time series of hourly VACM current meter data: Position E, depth 385 m; Jan, Apr 1982.

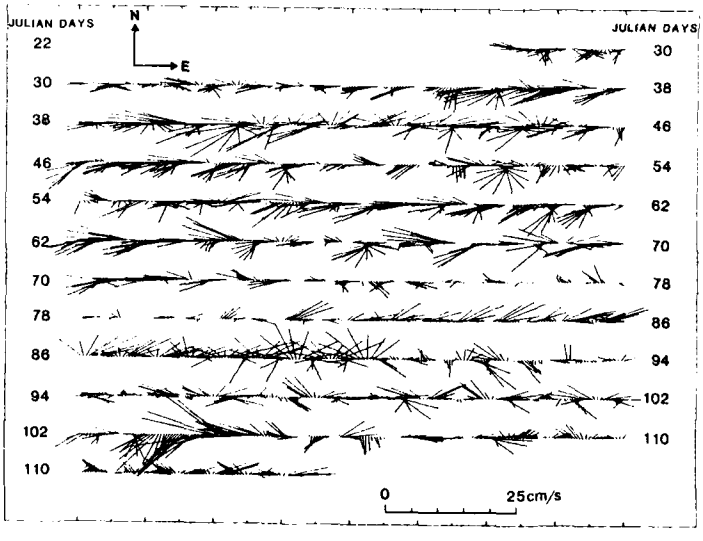

Fig. 15. Velocity vector time series of hourly VACM current meter data: Position E, depth 638 m; Jan, Apr 1982.

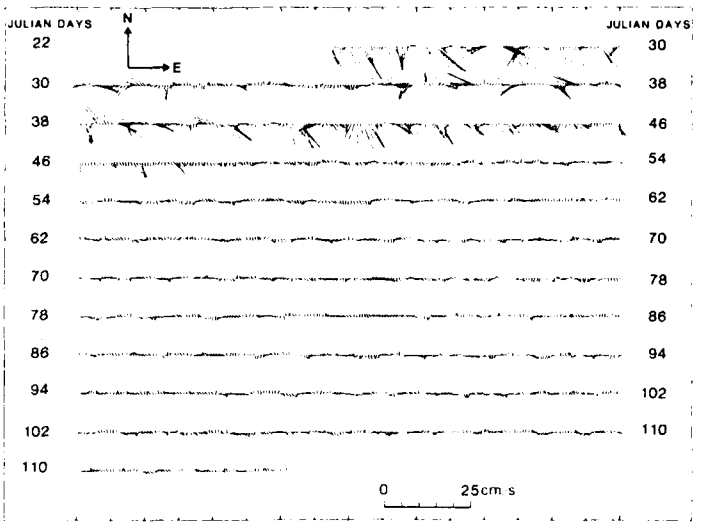

Fig. 16. Velocity vector time series of hourly NBA current meter data: Position F, depth 296 m; Jan, Apr 1982. [Amplitude measurements failed after day 46 and only direction is recorded. The current direction correlates well with the deep current meter (at 740 m) on the same mooring.]

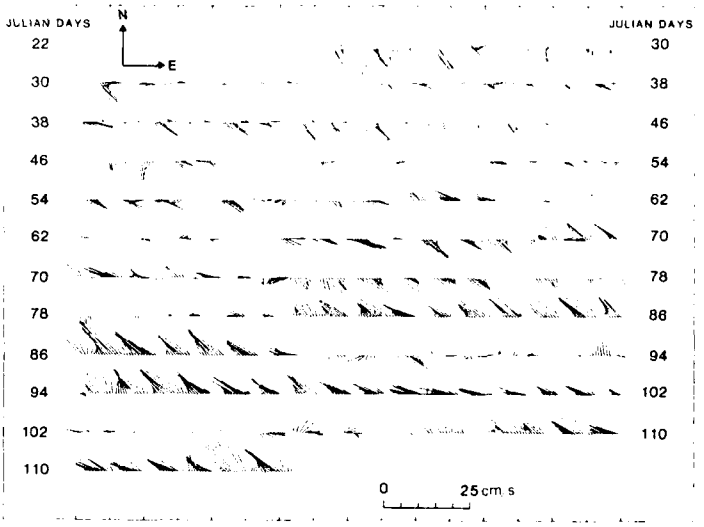

Fig. 17. Velocity vector time series of hourly VACM current meter data: Position F, depth 740 m; Jan, Apr 1982.

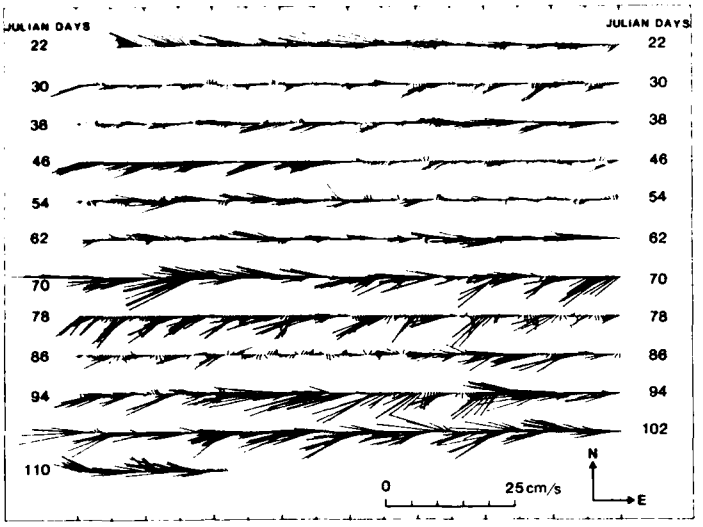

Fig. 18. Velocity vector time series of hourly NBA current meter data: Position G, depth 228 m; Jan, Apr 1982.

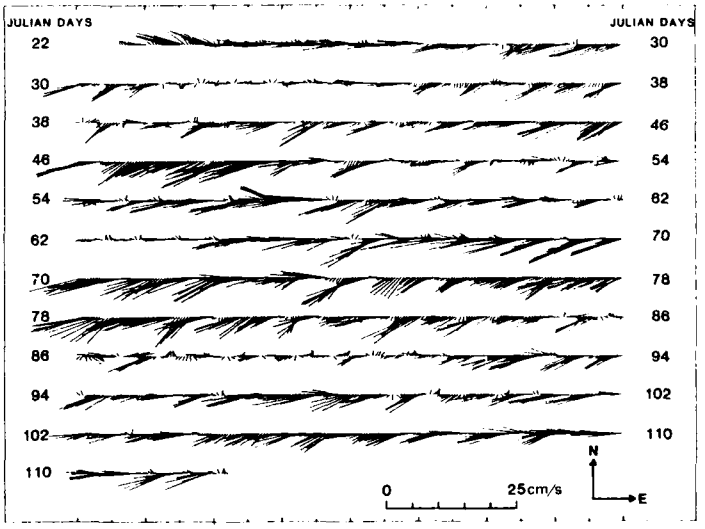

Fig. 19. Velocity vector time series of hourly NBA current meter data: Position G, depth 412 m; Jan, Apr 1982.

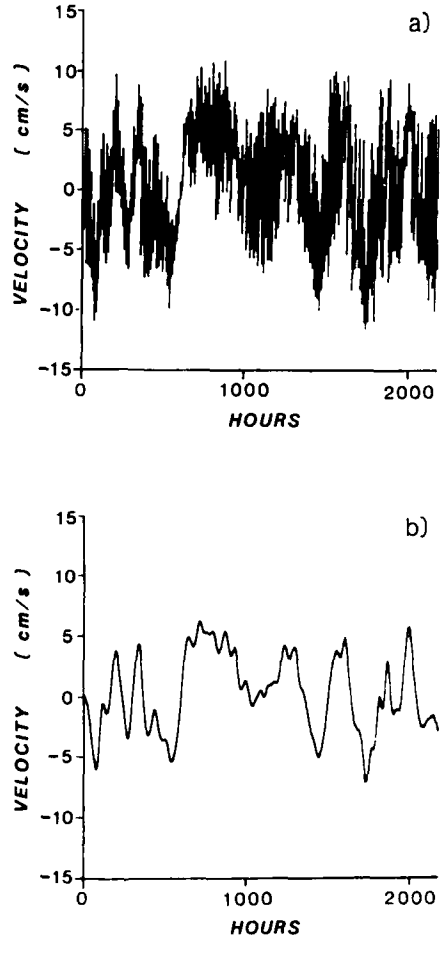

Fig. 20. Example of current meter data filtering: (a) hourly values of E-W component of velocity from NB acoustic current meter; spikes indicate the semidiurnal tides; (b) smooth version after filtration by Groves filter.

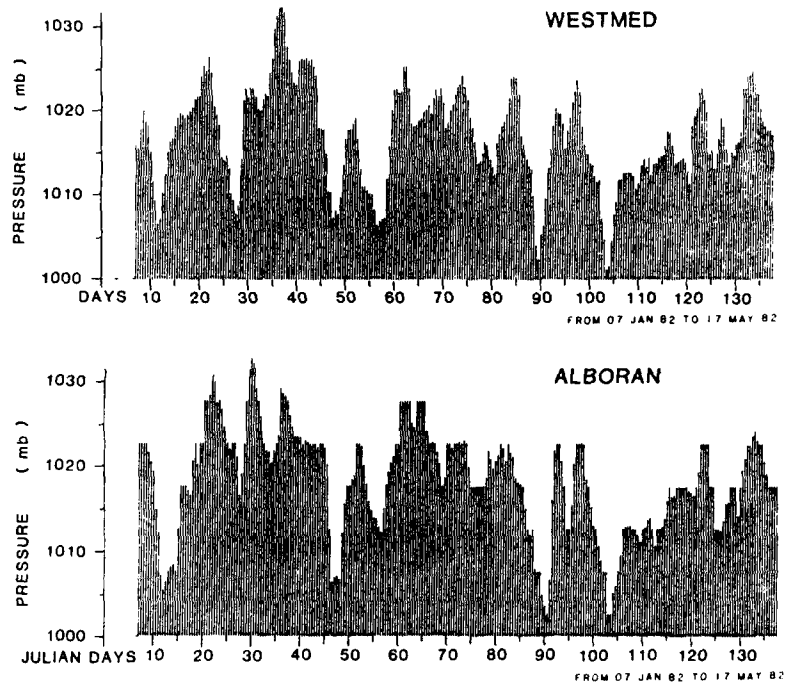

Fig. 21. Time series of atmospheric pressure in mbar. [WESTMED and ALBORAN signify the average atmospheric pressure computed over west Mediterranean Sea and Alboran Sea respectively.]

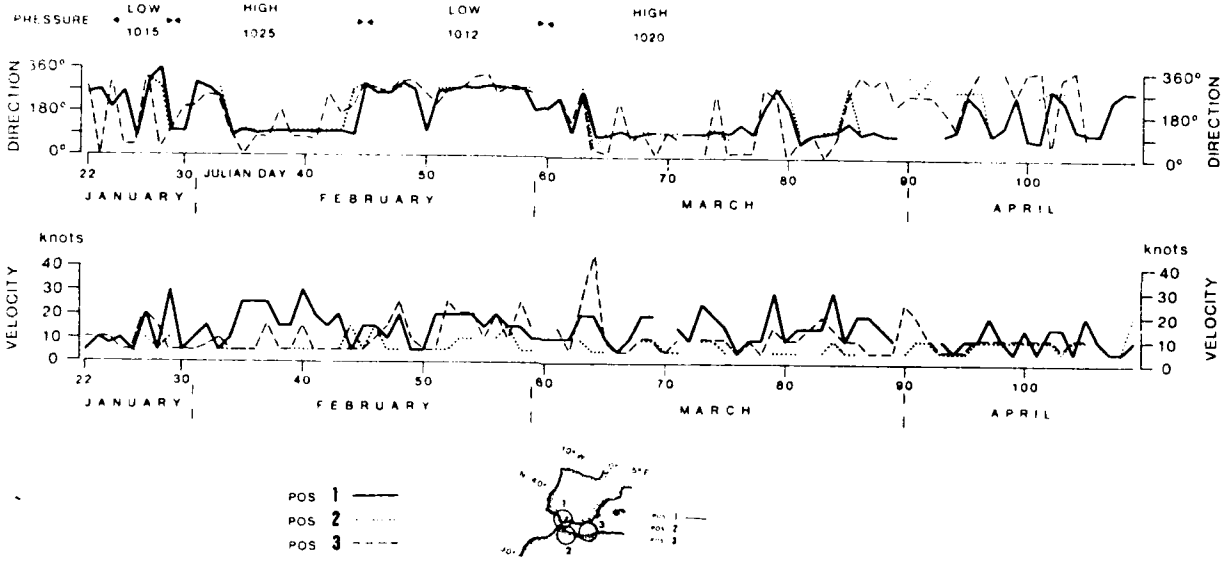

Fig. 22 — Wind amplitude and phase from three stations located near the Alboran Sea. [Data cover the period of oceanographic measurements. PRESSURE identifies the average of the average western Mediterranean pressure.]

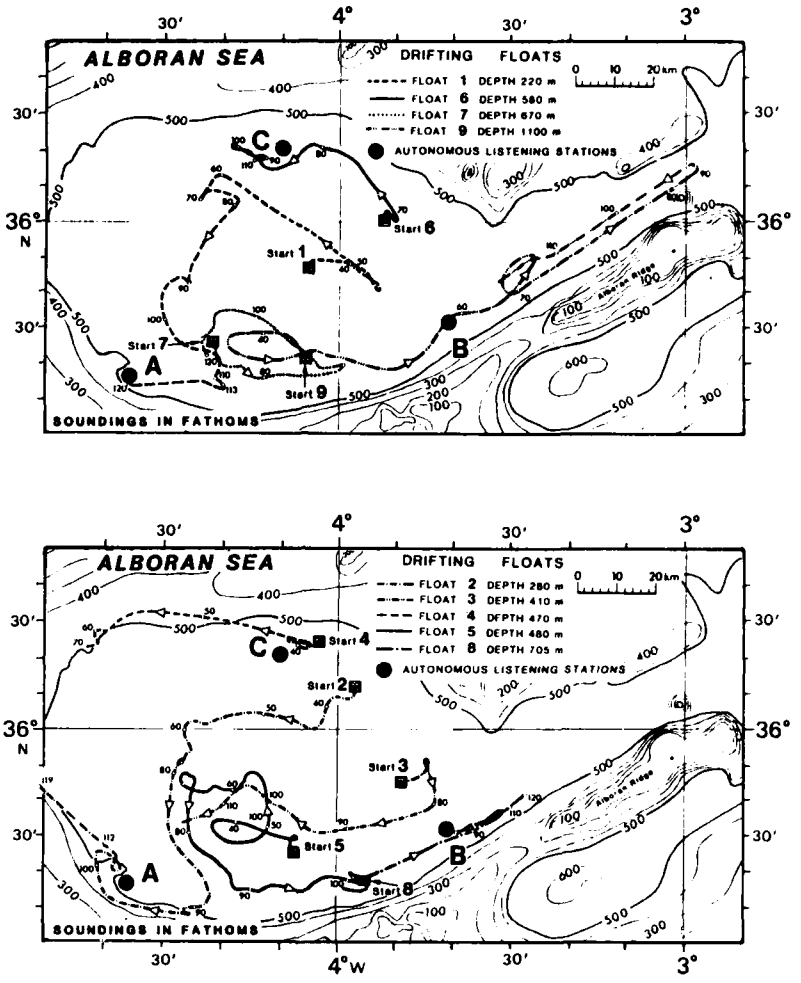

Fig. 23. Tracks of floats deployed in three months: (a) Floats 1, 6, 7, 9; (b) Floats 2, 3, 4, 5, 8. ['Start' indicates the starting point, and numbers near the tracks are Julian days. When float 9 moved east of B (days 75 to 109) it was shadowed from A and C and was tracked only by B. Float 6 at day 92 had a power loss in transmitted signal; later it was retrieved from near bottom after water had penetrated into the releaser. Positions at day 119 for Float 2 and at day 120 for Floats 1 and 8 were established from the shipboard receiver, because the autonomous listening stations at A, B and C had already been retrieved.]

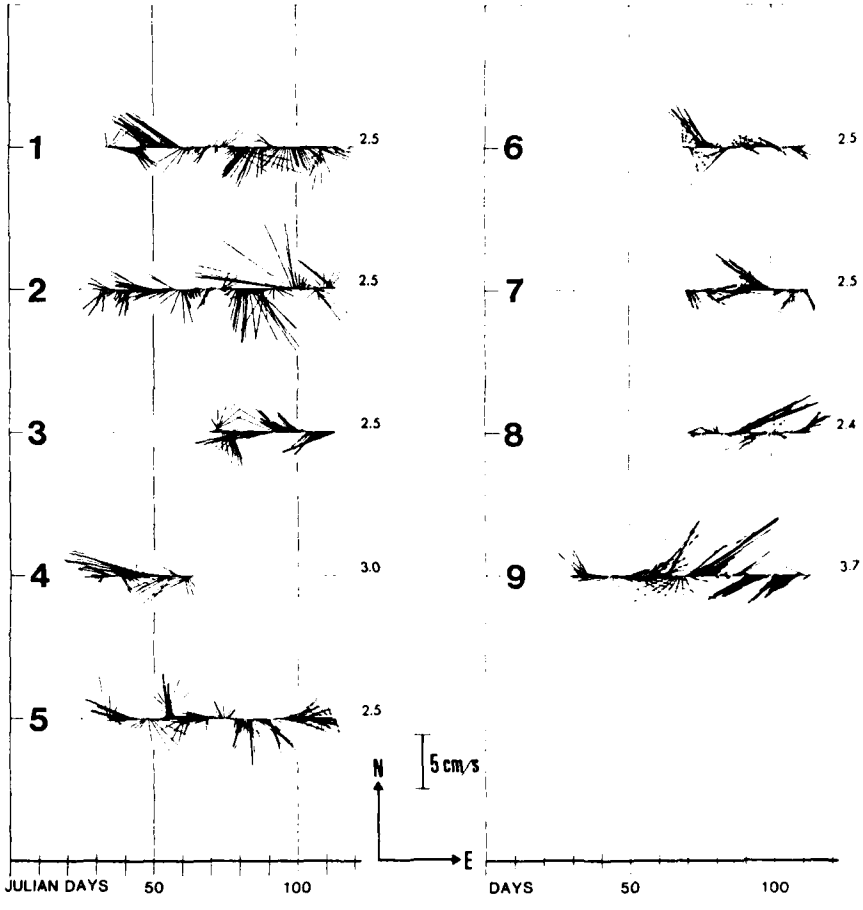

Fig. 24. Time series of 12-hourly velocity vectors for all floats. [The number on the left signifies the float number, and the number on the right signifies the average velocity amplitude in cm/s.]

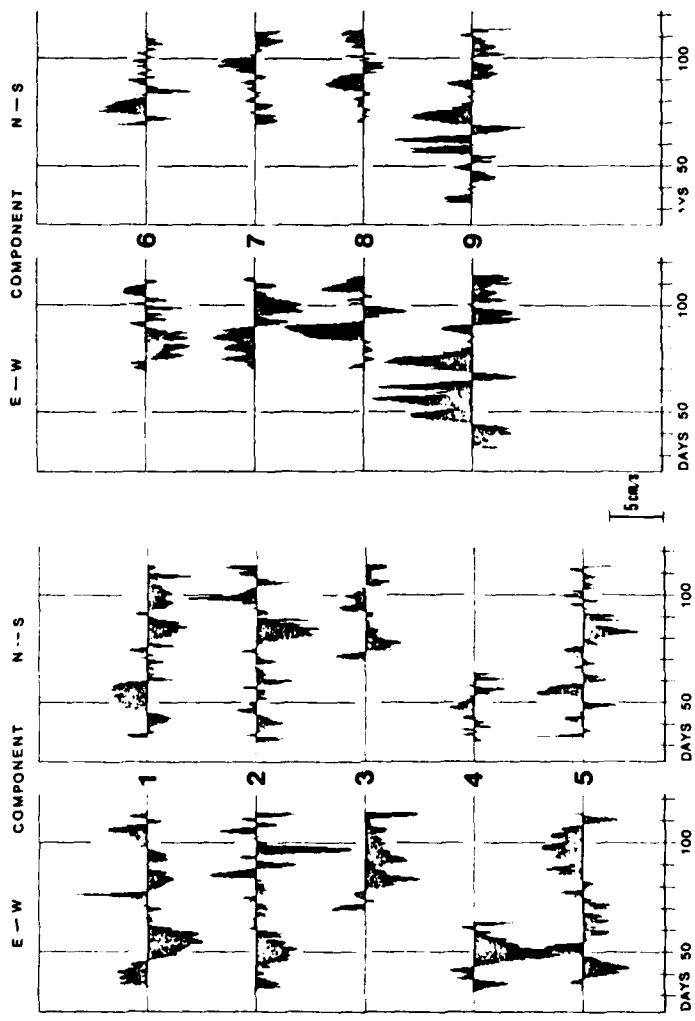

Fig. 25. Time series of 12-hourly velocity components for all floats. [Numbers signify the floats. E-W and N-S signify the east-west and north-south components (direction towards east and north being positive-up).]

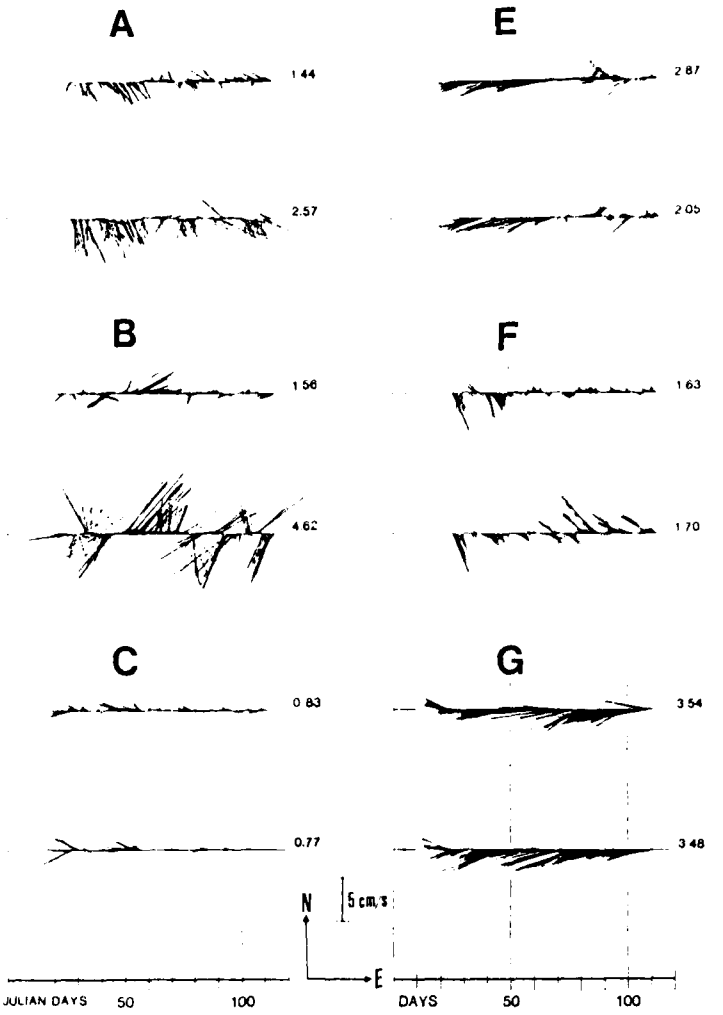

Fig. 26. Time series of 12-hourly current velocity vectors for all current meters. [Letters signify the moorings, upper time series is for current meter at 300 m depth, lower at 700 m; lower current meter at mooring G was only 400 m deep. Vertical lines in upper B and F indicate the time when malfunctioning of amplitude measurement started, measurement of direction is correct. Numbers on the right signify the average velocity amplitude in cm/s.]

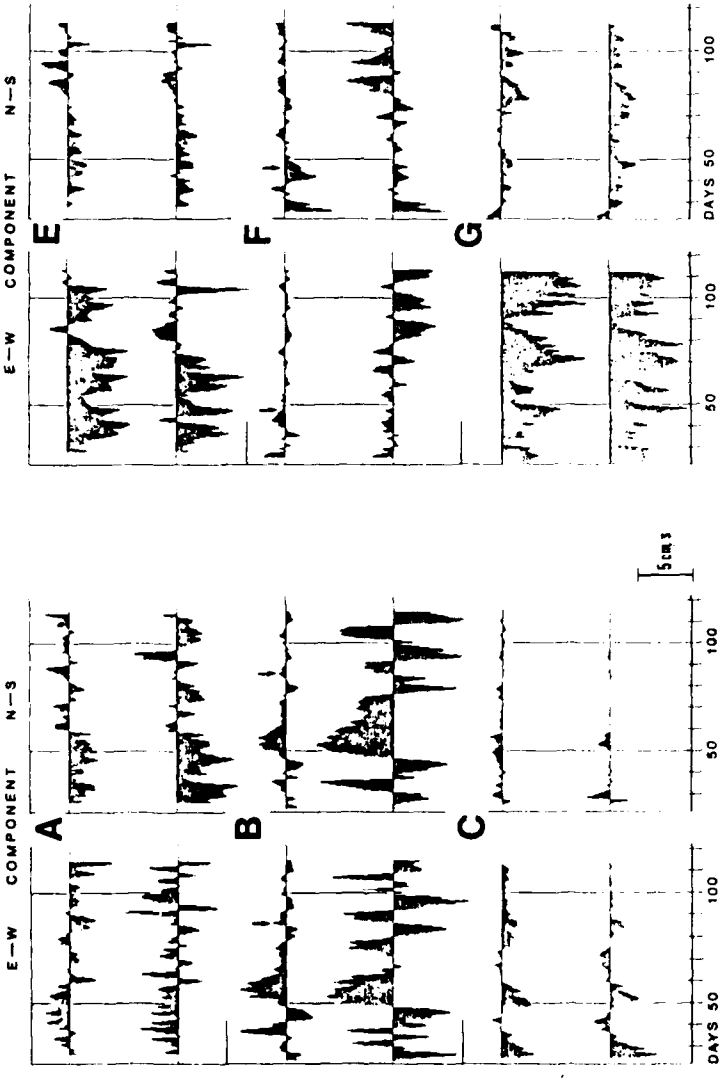

Fig. 27. Time series of 12-hourly current velocity components for all current meters. (Letters signify the moorings, upper time series is for current meter at 300 m depth, lower at 700 m. Lower current meter at mooring G was only 400 m deep. E-W and N-S signify east-west and north-south components (direction towards east and north being positive-up). Malfunctioning of amplitude in upper B and F started on Julian day 71 and 46, respectively, direction is correct.)

intentionally blank page

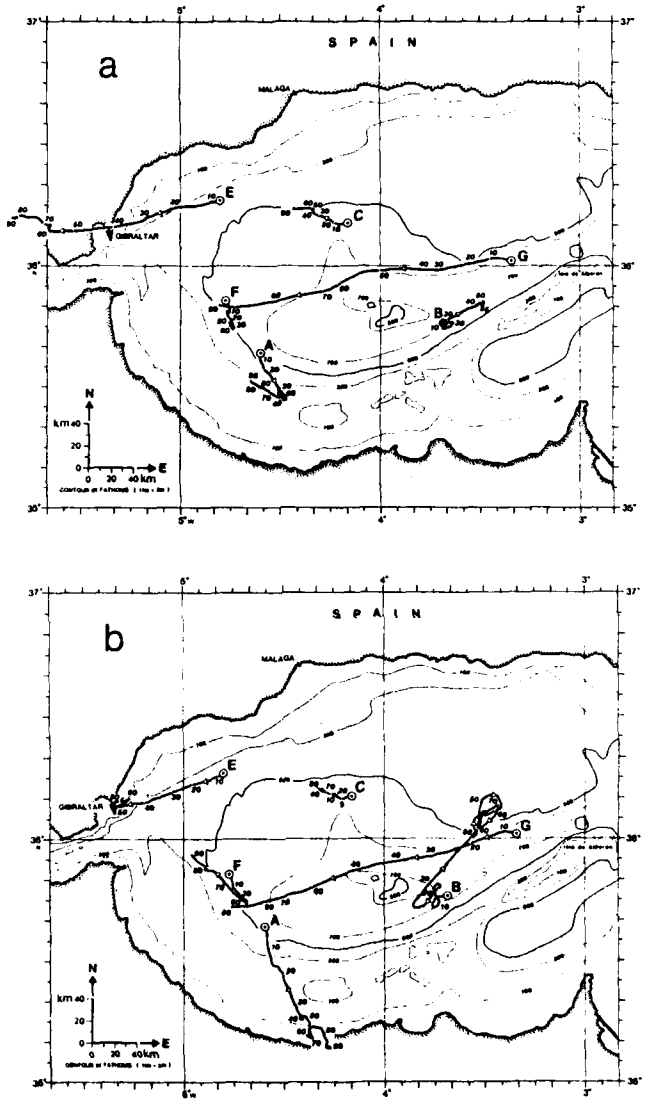

Fig. 28. Progressive vector diagrams for current meters (starting at Julian day 22 hours 00): (a) current meters at about 300 m depth; (b) current meters at about 700 m depth. [Lower current meter at mooring G was only 400 m deep. Numbers near tracks signify Julian days. Tracks are shorter for upper B and F because the current meters malfunctioned later.]

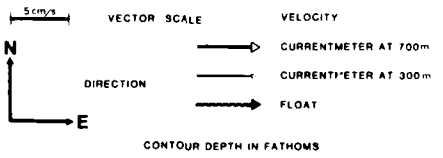

Fig. 29. Two-day current vector field created from float and current meter data. [Numbers signify Julian days.]

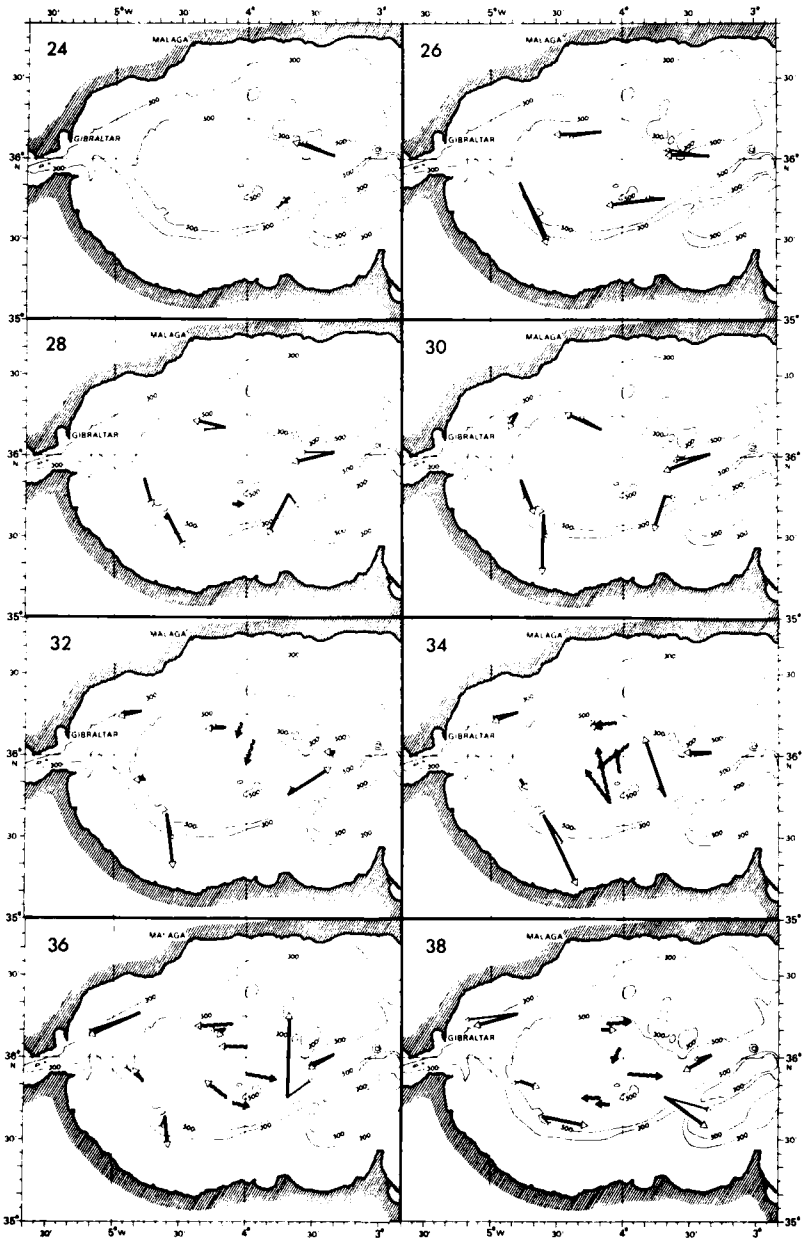
24
26
28
30
32
34
36
38
MALAGA
GIBRALTAR

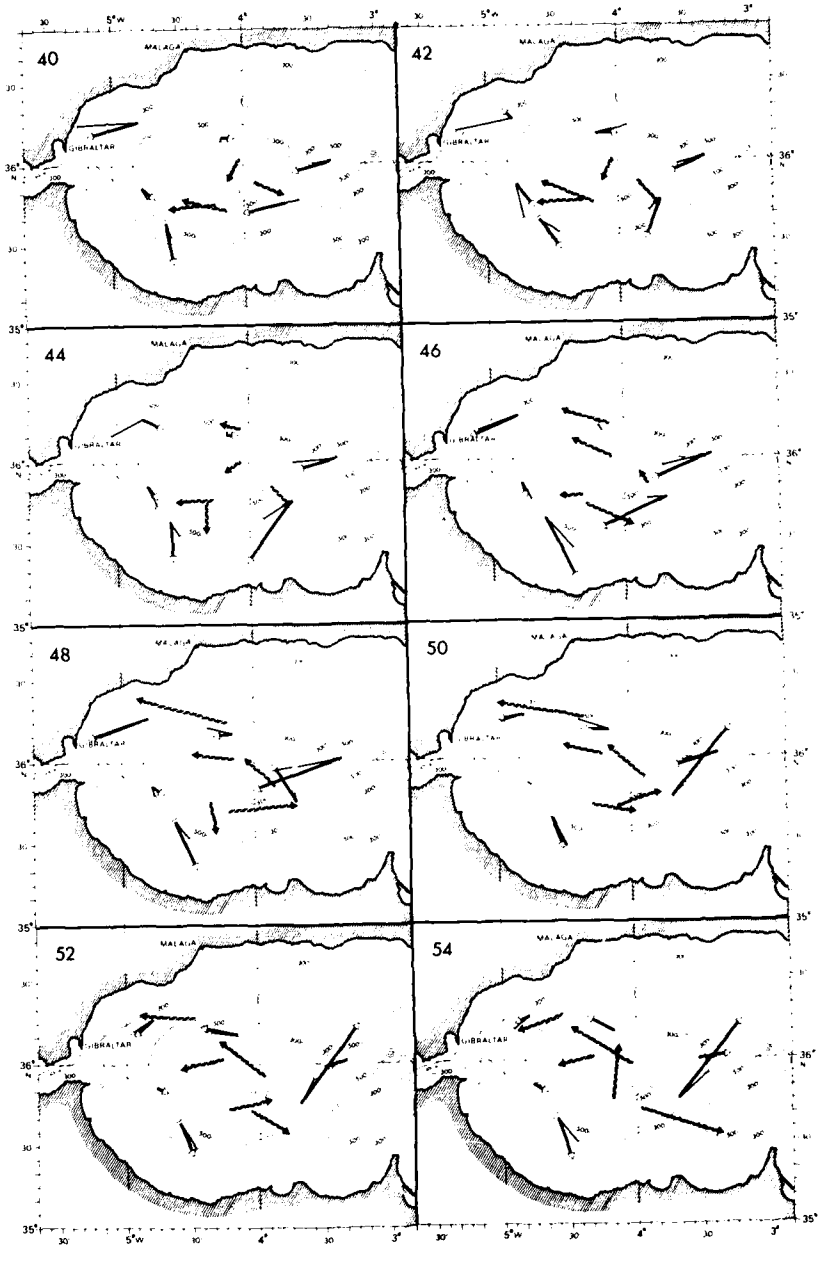

Fig. 29 continuation 1.

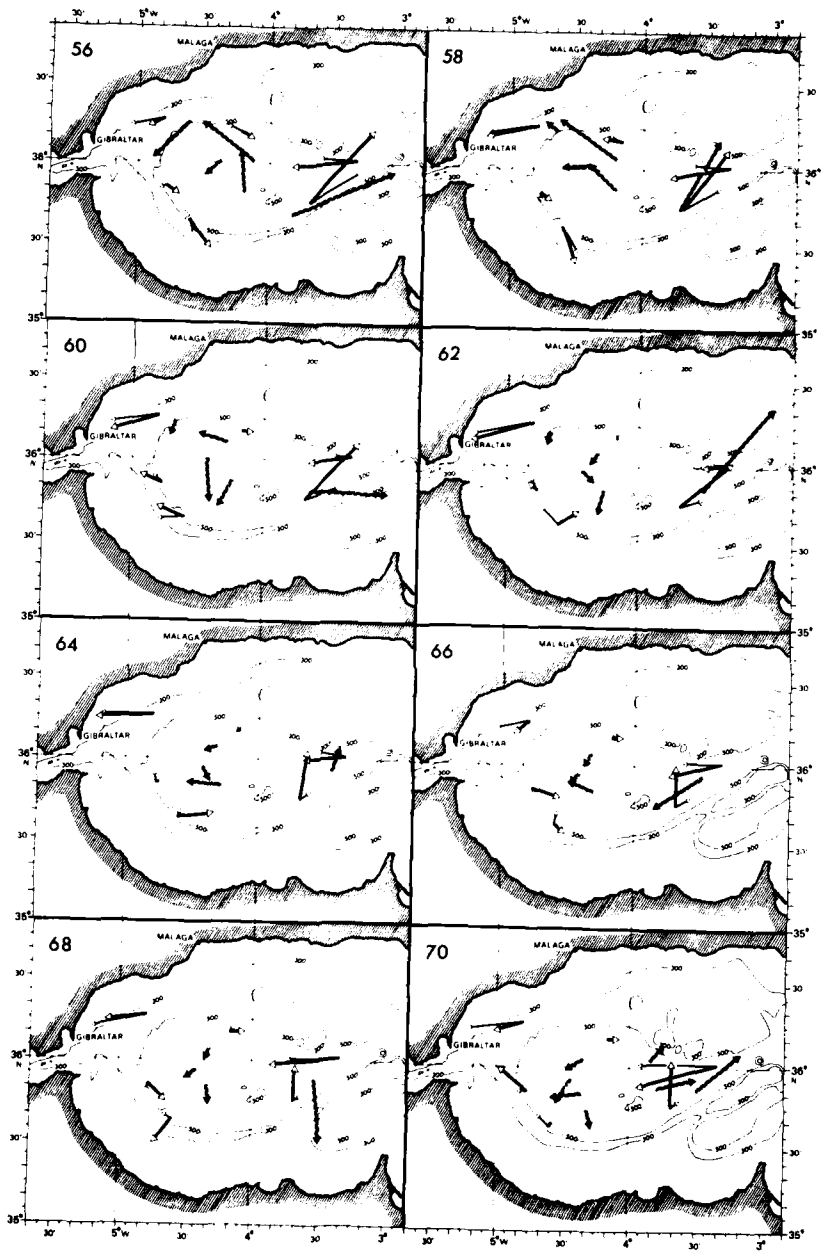

Fig. 29 - continuation 2.

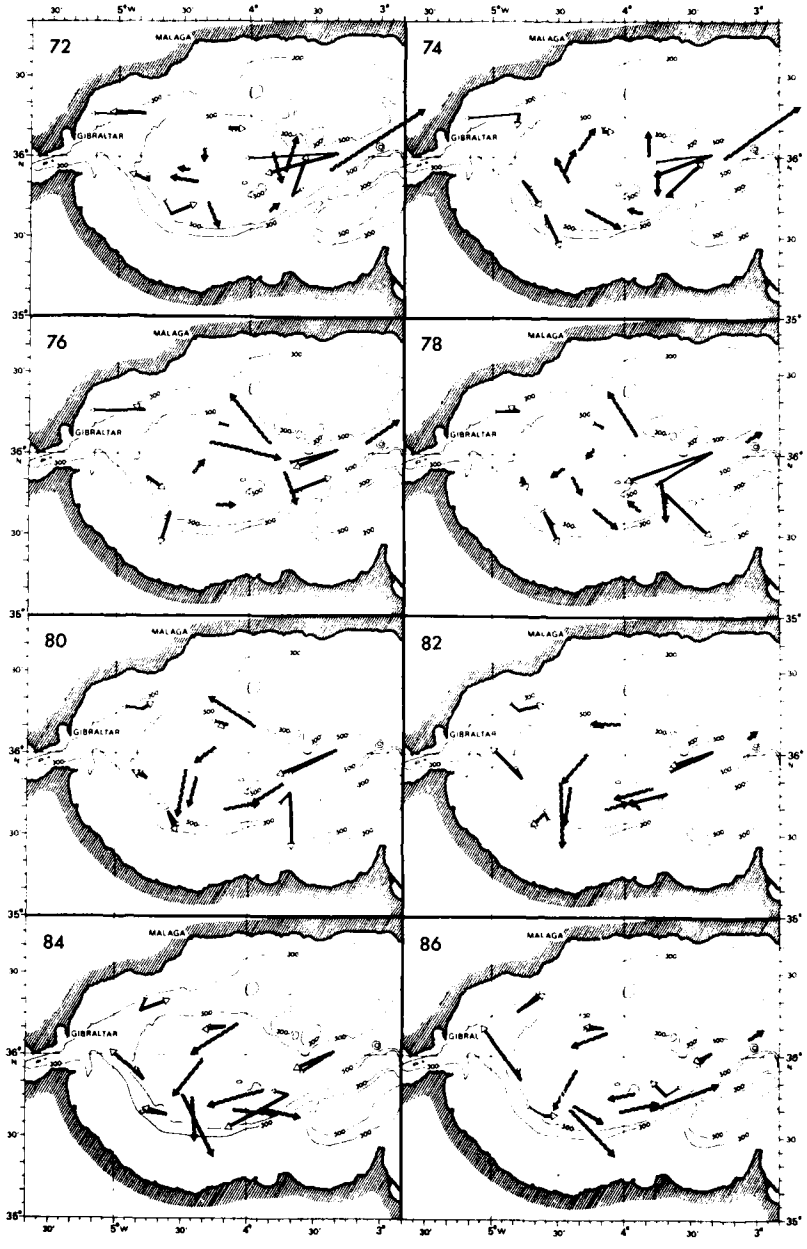

Fig. 29 - continuation 3.

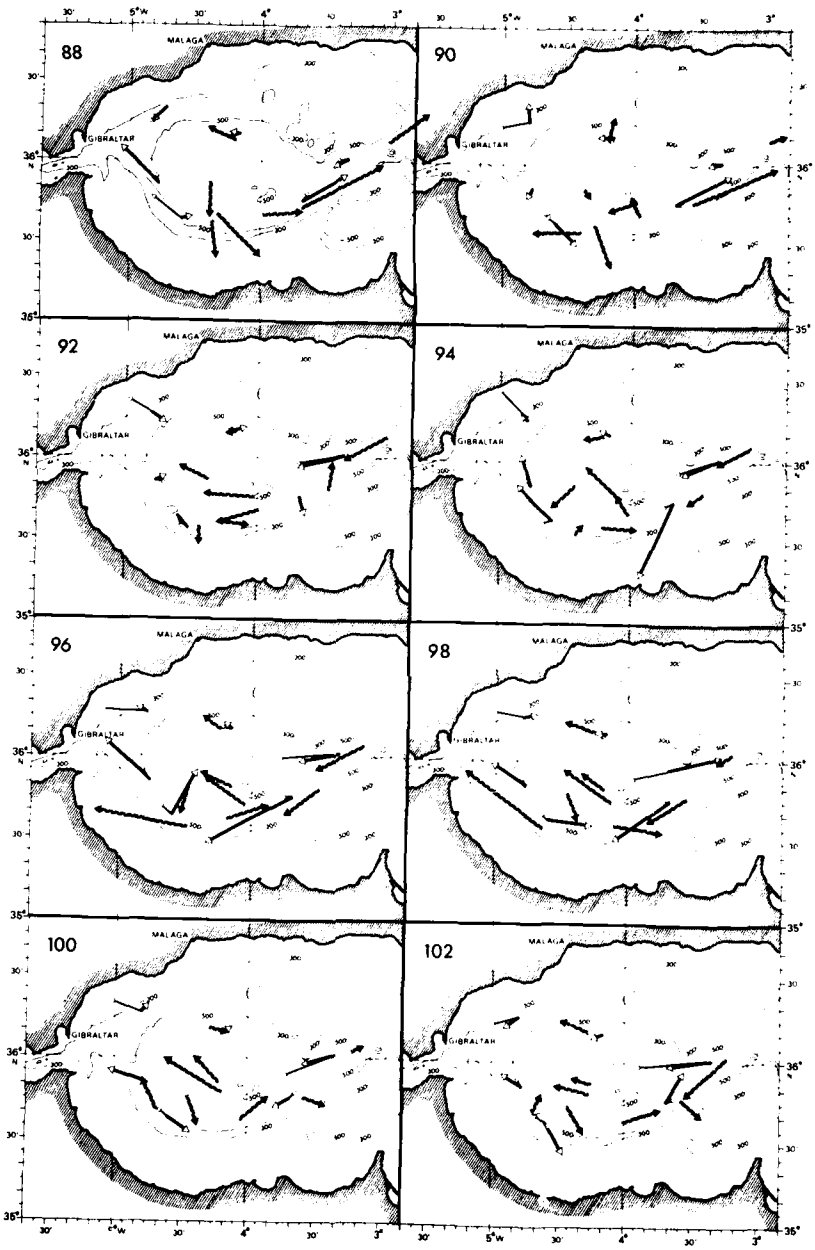

Fig. 29 continuation 4.

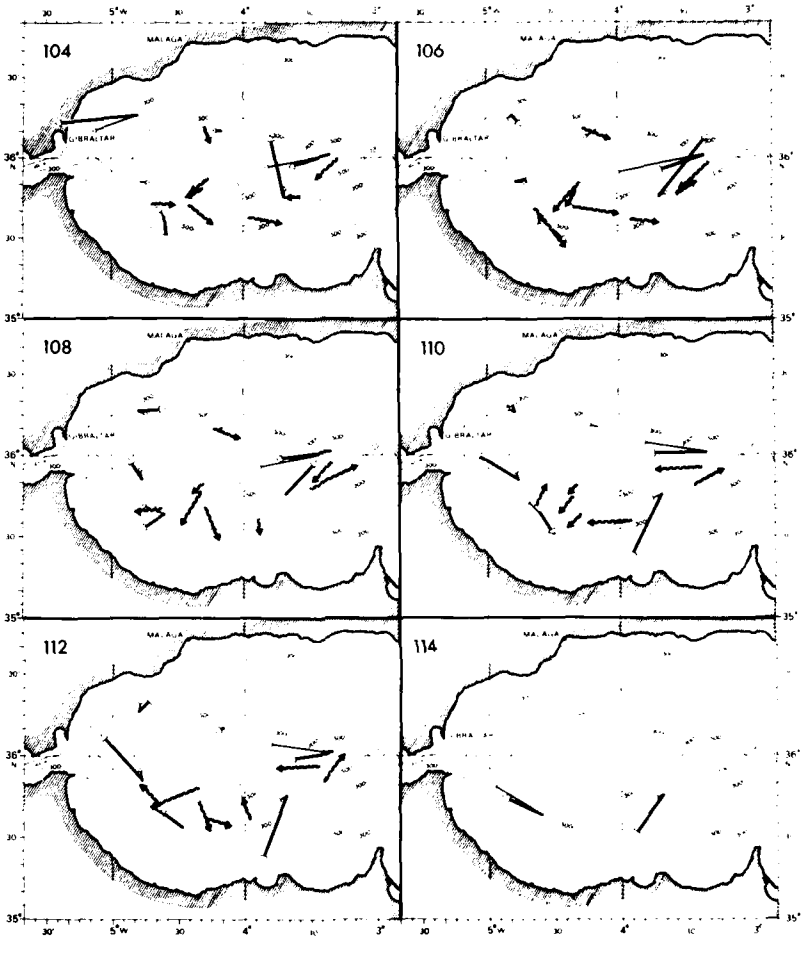

Fig. 29 continuation 5

Fig. 30. Time and space change of circulation. [Six time windows were chosen. Time interval was 400 h and is marked by numbers showing the time lapse in hours from 0000 h on 20 Jan. Progressive vector diagram for current meter data, and tracks for floats in corresponding period are shown: upper current meters current meters at about 300 m; lower current meters current meters at about 700 m, floats float tracks. A, B, C, E, F, G are the mooring positions. Lower current meter at G was only 400 m deep.]

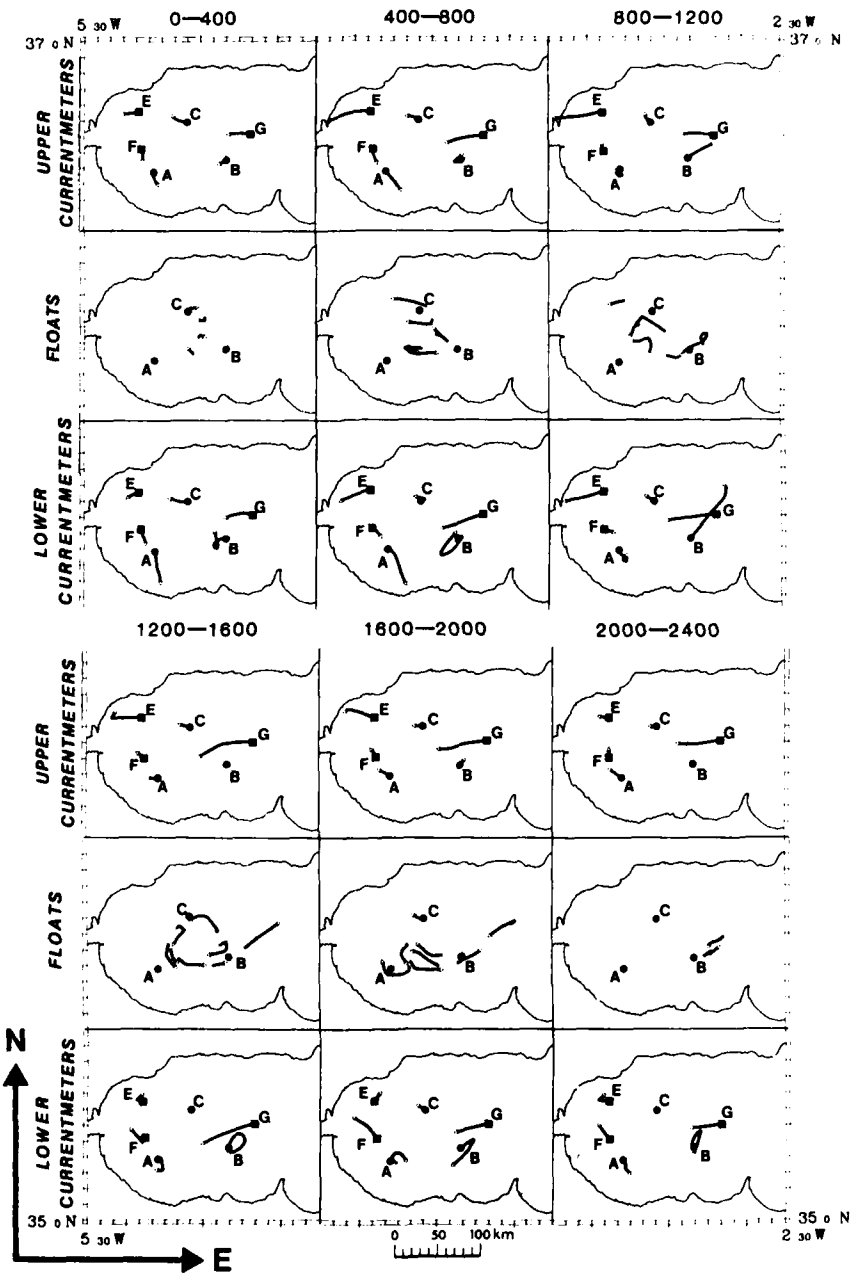
0—400
400—800
800—1200
1200—1600
1600—2000
2000—2400
5 30 W
2 30 W
37 0 N
35 0 N
UPPER CURRENTMETERS
FLOATS
LOWER CURRENTMETERS
A
B
C
E
F
G
N
E
0 50 100 km

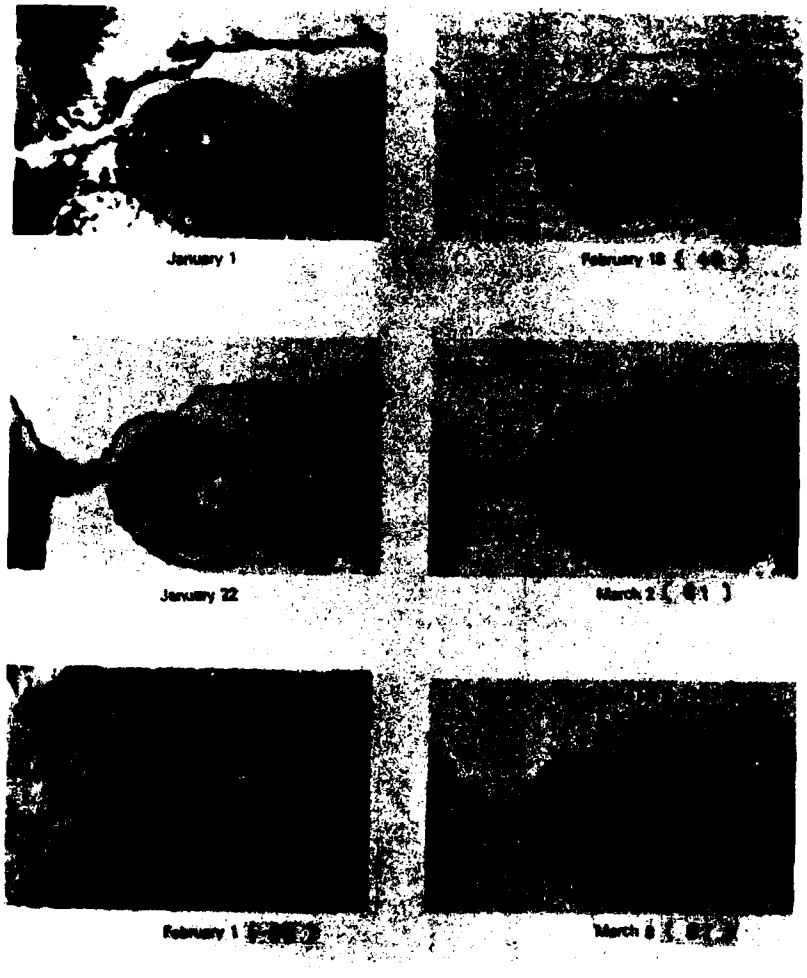

Fig. 31 Satellite infrared images of sea-surface temperature, NOAA 7 (from La Violette, NORDA). [Considerable variability is visible, agreement with CTD is good.]

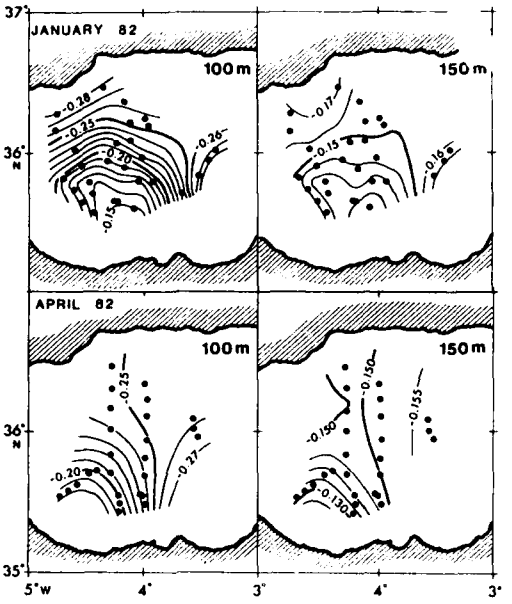

Fig. 32. Contours of dynamic height anomaly in dynamic meters for the depths of 100 and 150 m (relative to 200 m) from January and April 1982. [They show broad anticyclonic circulation. Dots signify the positions of CDT casts.]

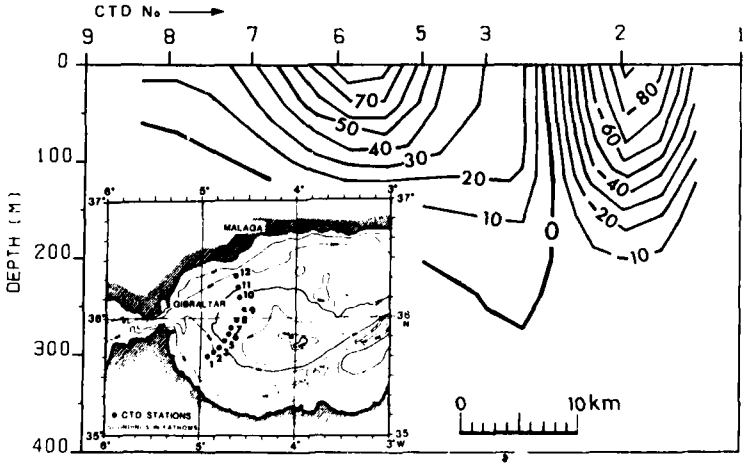

Fig. 33. Cross-section of computed geostrophic current in cm/s from March 1982: CTD stations are indicated in map; level of no motion at 200 m.

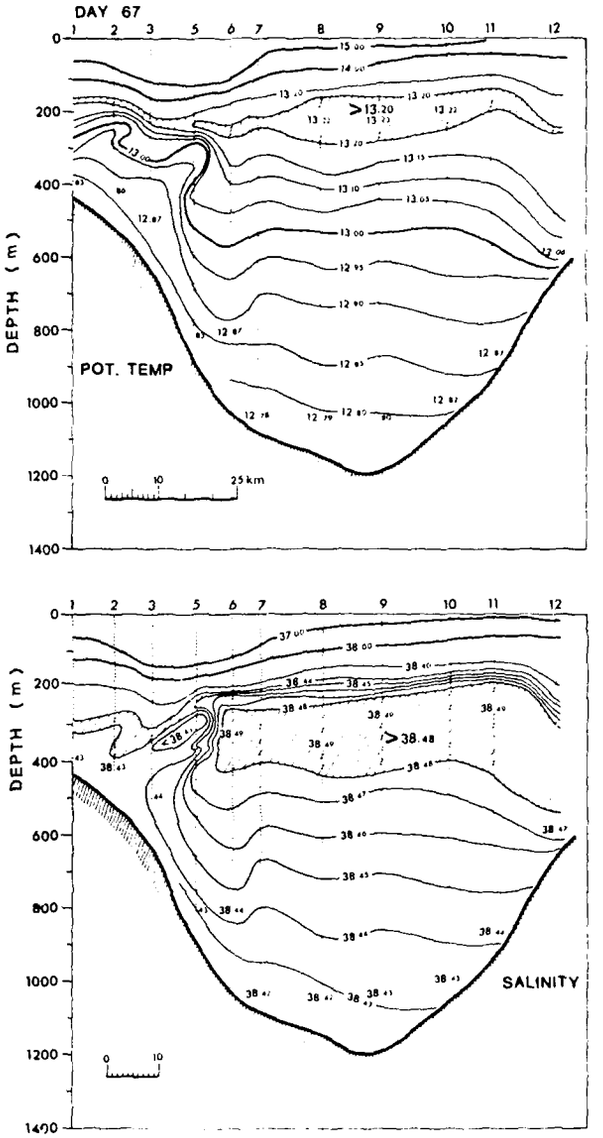

Fig. 34. Cross-section of potential temperature and salinity: CTD, cruise March 1982. [The isolines bend up towards the Moroccan continental slope. Very intense upwelling and mixing is visible.]

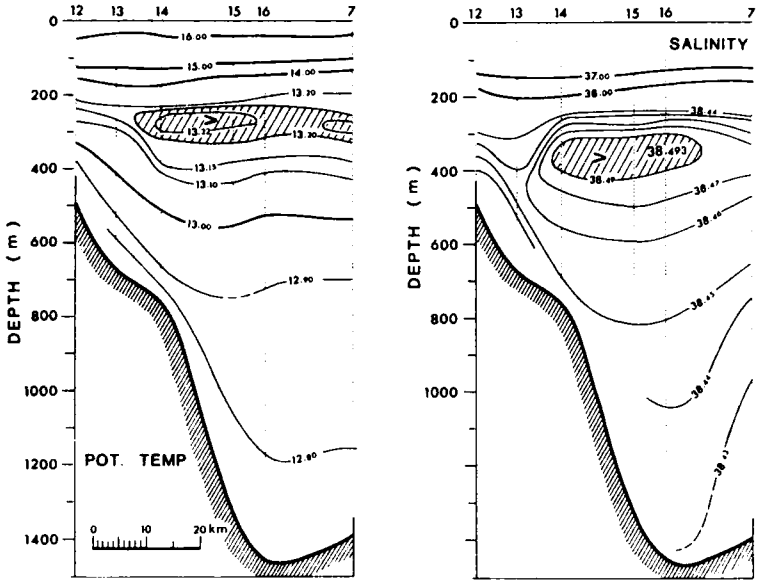

Fig. 35. Cross-section of potential temperature and salinity: CTD, cruise April 1982. [The isolines bend up towards the Moroccan continental slope.]

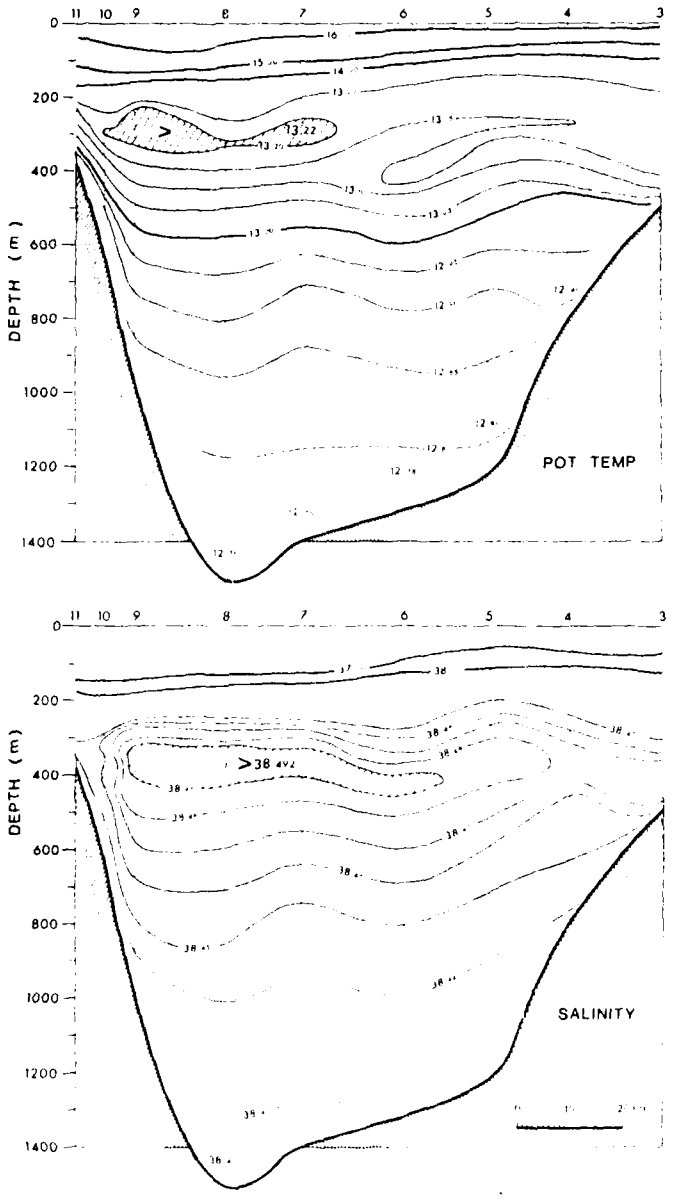

Fig. 36. Cross-section of potential temperature and salinity. CTD, cruise April 1982. [The isolines bend up towards the Moroccan continental slope, Levantine water-mass is concentrated in the southern part of Alboran basin.]

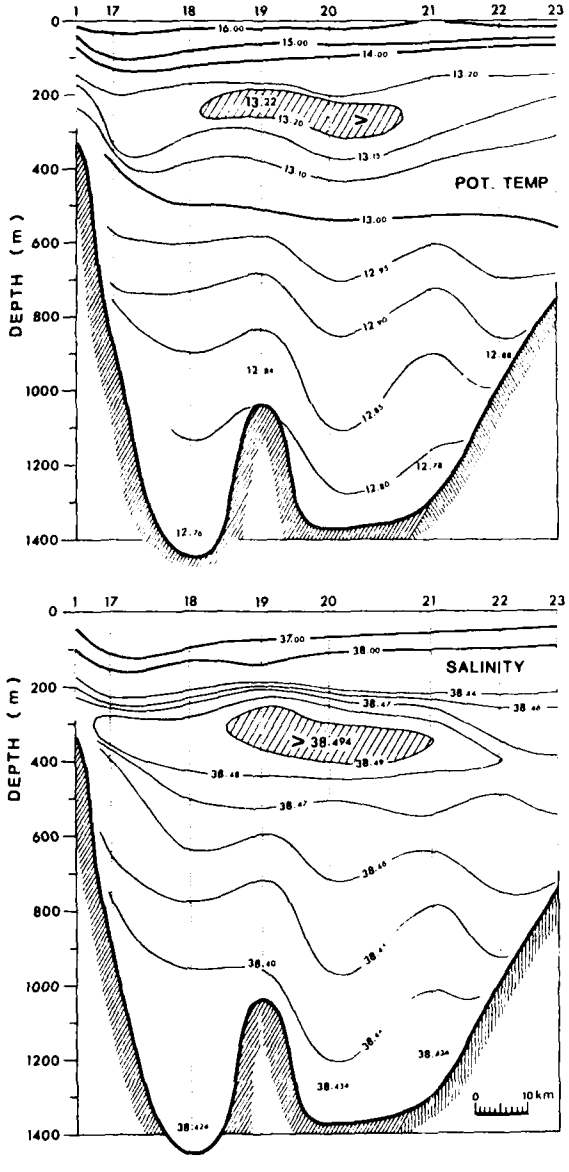

Fig. 37. Cross-section of potential temperature and salinity: CTD, cruise April 1982. [Weak bending up of isolines towards the Moroccan continental slope is visible. The effect is less pronounced than in sections located to the west Levantine water-mass is concentrated in the middle of Alboran basin.]

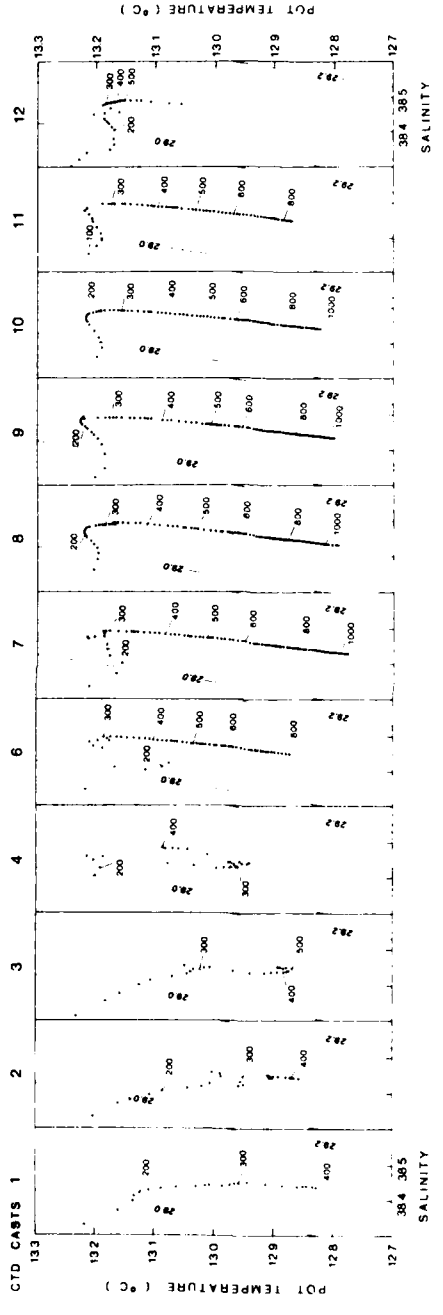

Fig. 38. Potential temperature/salinity diagrams for CTD cross-section from Fig. 34. [Mixing is very visible. Levantine water maximum is already at the depth of 200 m.]

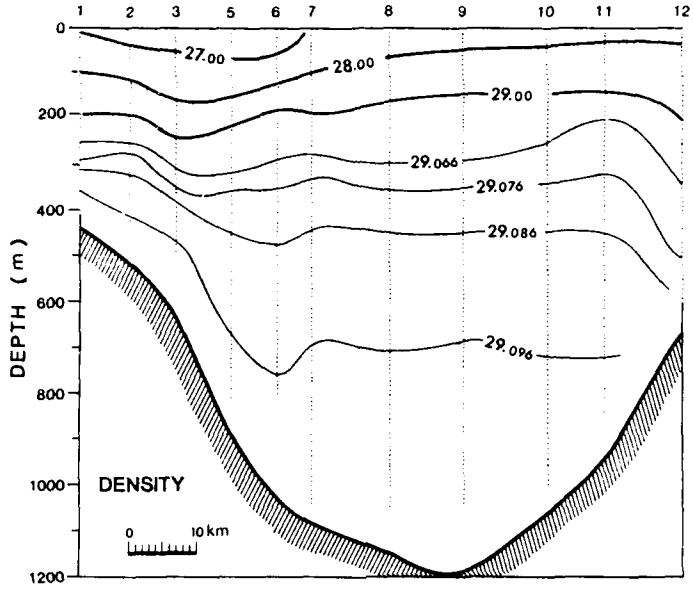

Fig. 39. Potential sigma for CTD cross-section from Fig. 34. [Variation in density is small and bending up of isopycnals towards the Moroccan continental slope is visible.]

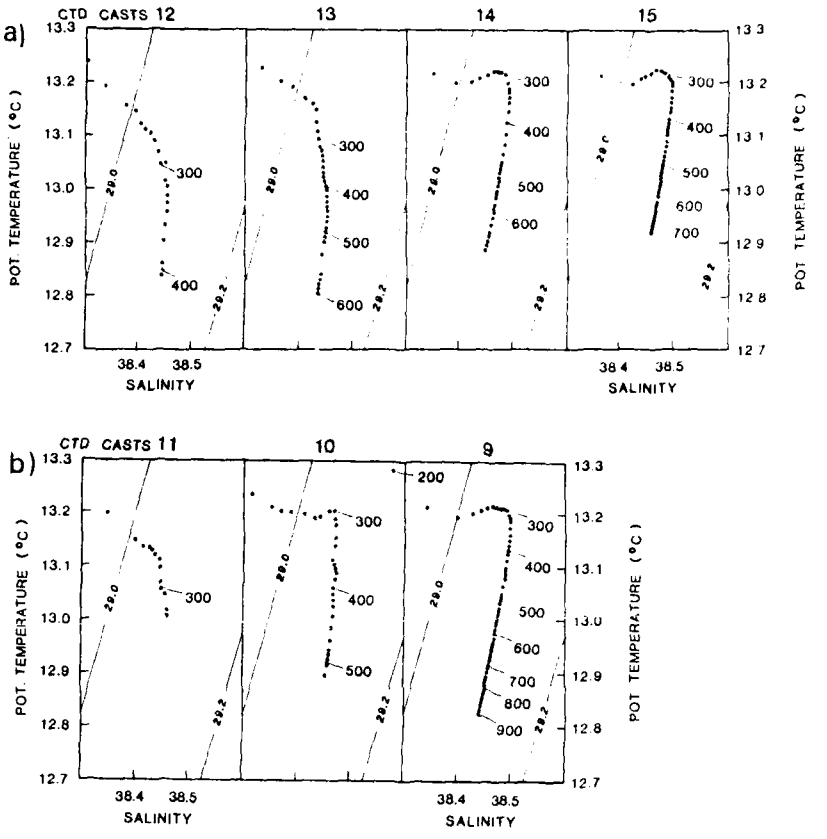

Fig. 40. Potential temperature/salinity diagrams for CTD cross-sections: (a) cross section from Fig. 35; (b) cross section from Fig. 36.

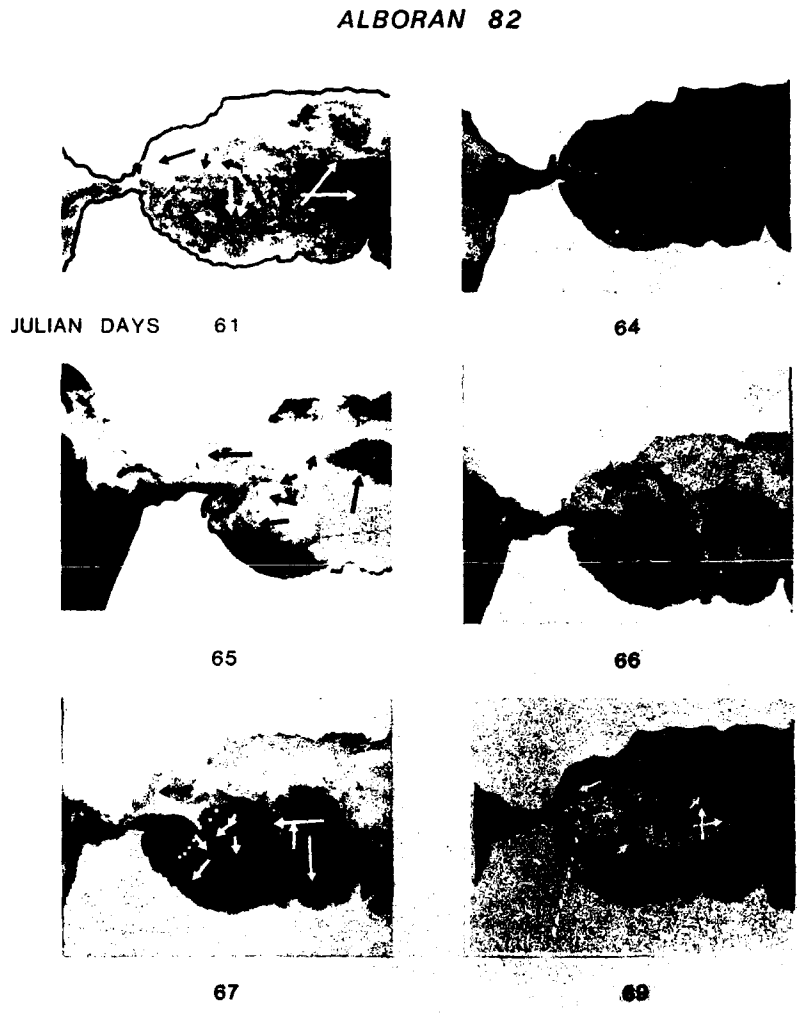

Fig. 41. Satellite infrared images demonstrating the growth of a new vortex. (Numbers indicate Julian day. Arrows indicate current vectors obtained from floats and current meters (at 700 m). Dots indicate CTD casts shown at cross-section in Fig. 34. Images from NOAA-7 were developed at SACLANTCEN by Böhm.)

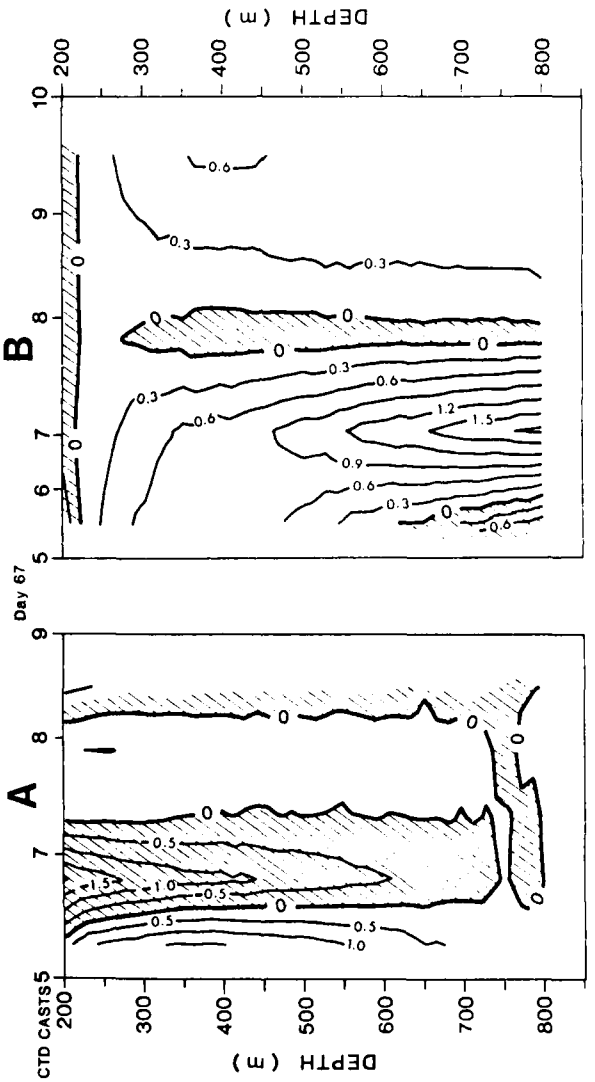

Fig. 42. Geostrophic current cross-section computed from CTD casts in Fig. 34. [Numbers signify the current speed in cm/s: (a) level of no motion at 800 m; (b) level of no motion at 220 m.]

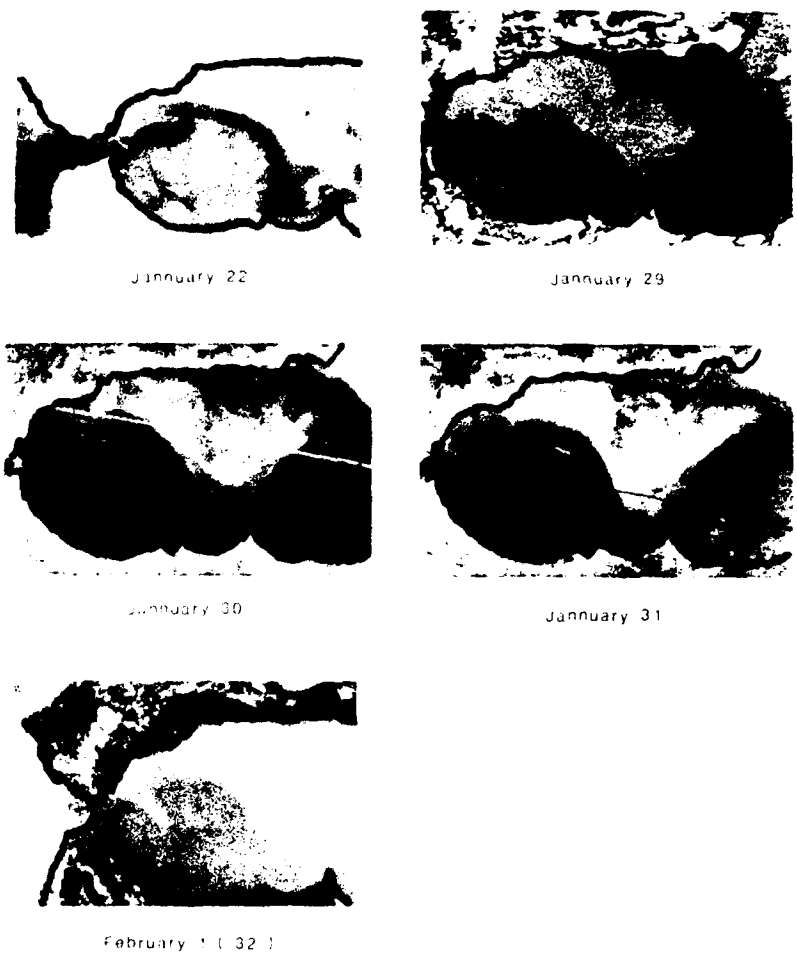

Fig. 43. Satellite infrared images of sea surface temperature from NOAA-7. [Sequence of these images is correlated with wind and pressure data. Numbers signify Julian day. Images were developed in SACLANTCEN by Wannamaker.]

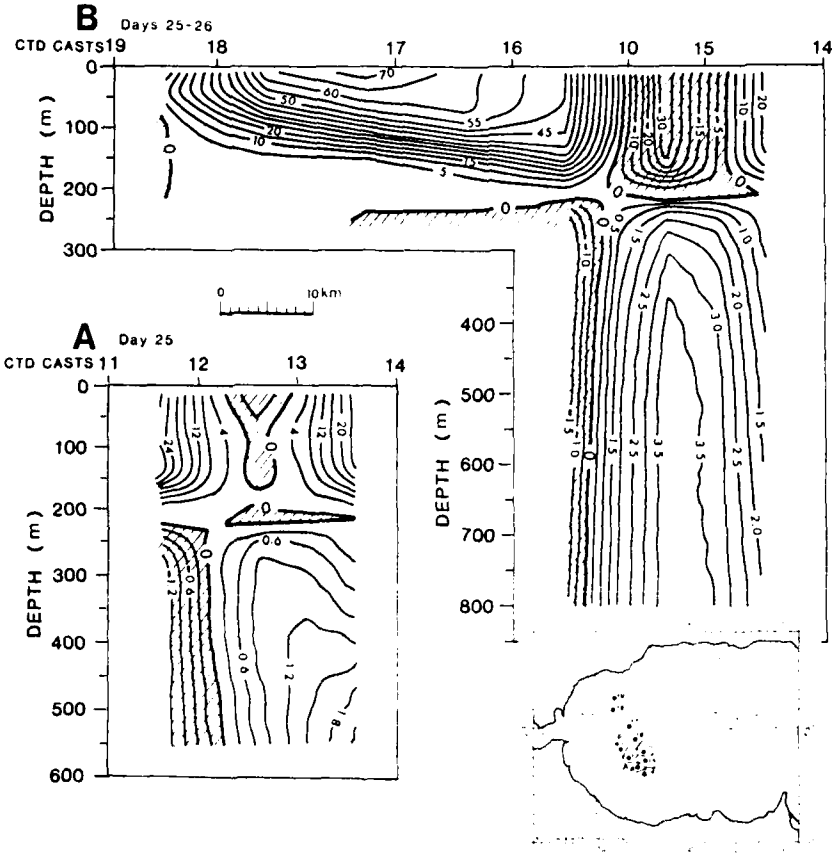

Fig. 44. Geostrophic current cross-section computed from CTD casts, cruise, January, 82. (Level of no motion at 220 m. Numbers signify the current speed in cm/s. Schematic in the lower left corner shows the position of the CTD stations and the deep circulation. Cyclonic motion is in agreement with the current meter data. (a) cross-section CTDs 11 to 14; (b) cross-section CTDs 14 to 19.)

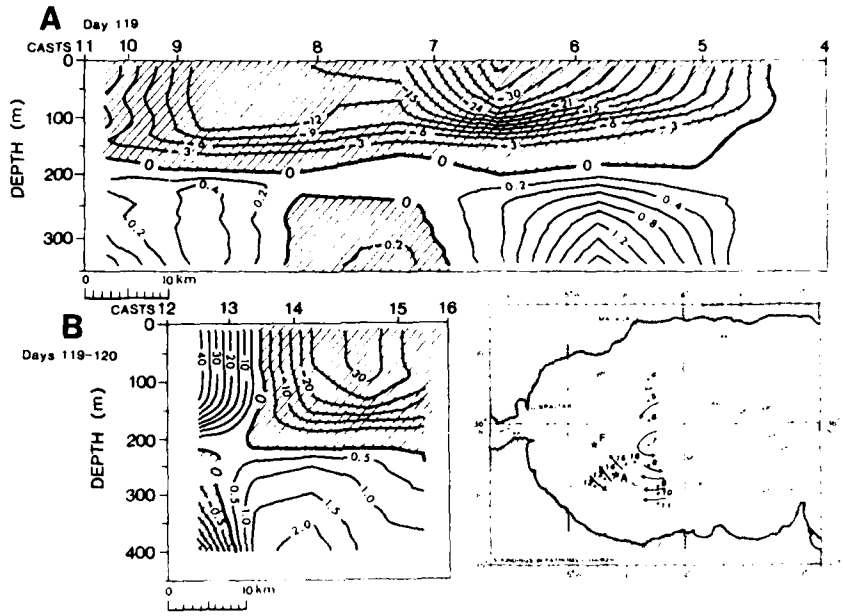

Fig. 45. Geostrophic current cross-section computed from CTD casts, cruise, April, 82 [Level of no motion at 220 m. Numbers signify the current speed in cm/s. Schematic in the lower left corner shows the positions of CTD stations and the deep circulation. Cyclonic motion in deep layer is in agreement with the current meter data. Surface layer shows the broad anticyclonic circulation. (a) cross-section CTDs 4 to 11, (b) cross-section CTDs 12 to 16.]

intentionally blank page

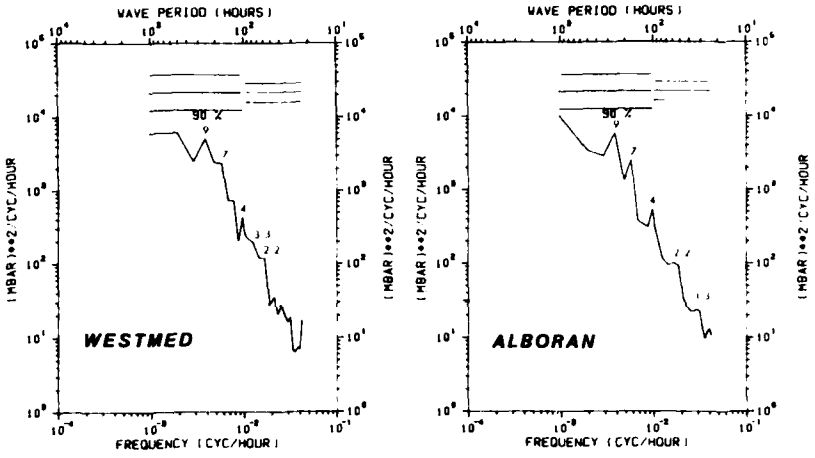

Fig. 46 Autospectra of atmospheric pressure. [WESTMED and ALBORAN signify the time series used for spectral estimation. 90% confidence level for gaussian distribution is shown. Numbers near peaks signify the periods in days.]

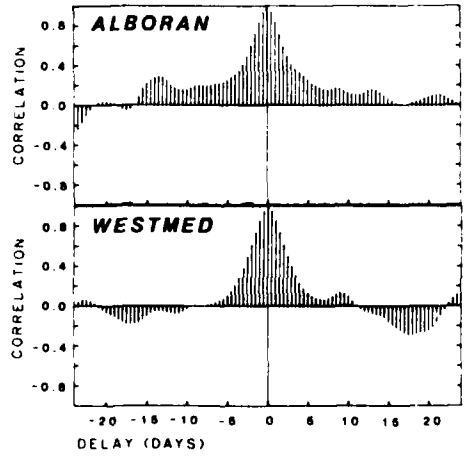

Fig. 47 Autocorrelation of atmospheric pressure. [WESTMED and ALBORAN signify the time series used in computation. Repetitive peaks show the low-frequency periodicities.]

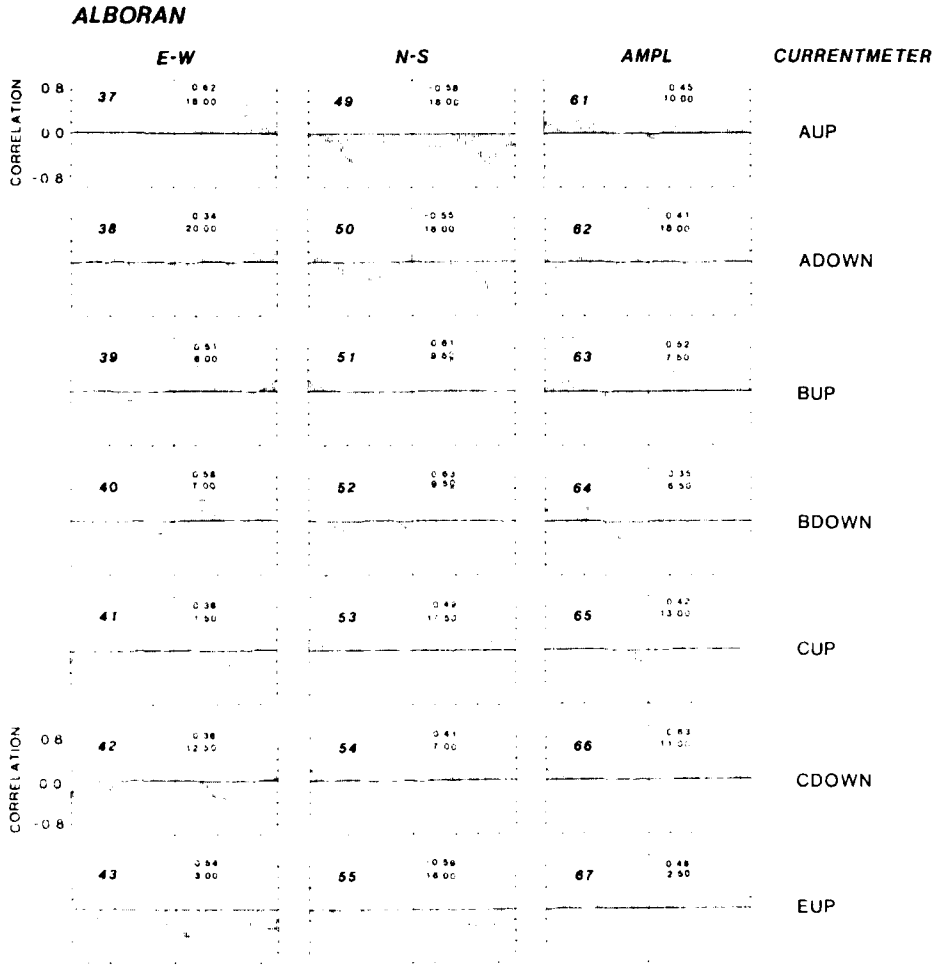
ALBORAN
E-W
N-S
AMPL
CURRENTMETER
CORRELATION
0.8
0.0
-0.8
37
0.62
18.00
49
-0.58
18.00
61
0.45
10.00
AUP
38
0.34
20.00
50
-0.55
18.00
62
0.41
18.00
ADOWN
39
0.51
8.00
51
0.61
9.50
63
0.52
7.50
BUP
40
0.58
7.00
52
0.63
9.50
64
0.35
6.50
BDOWN
41
0.38
1.50
53
0.49
17.50
65
0.42
13.00
CUP
CORRELATION
0.8
0.0
-0.8
42
0.36
12.50
54
0.41
7.00
66
0.83
11.00
CDOWN
43
0.54
3.00
55
-0.56
16.00
67
0.48
2.50
EUP

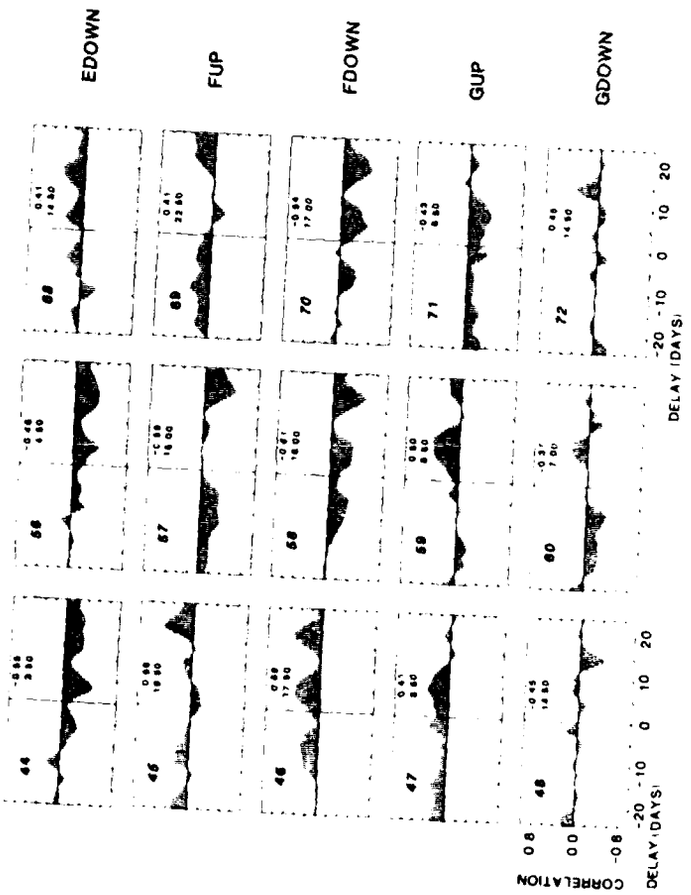

Fig. 48. Cross-correlation between current and average atmospheric pressure over Alboran Sea (ALBORAN). (Delay, in days, signifies the time-shift of current meter data relative in the pressure. Current meters are identified on the right side. UP and DOWN signifies the current meter at 300 m and 700 m, respectively. E-W, N-S signify east-west, north-south current velocity components and AMPL is the current speed. Numbers in each graph signify the highest cross-correlation and the corresponding delay in hours.)

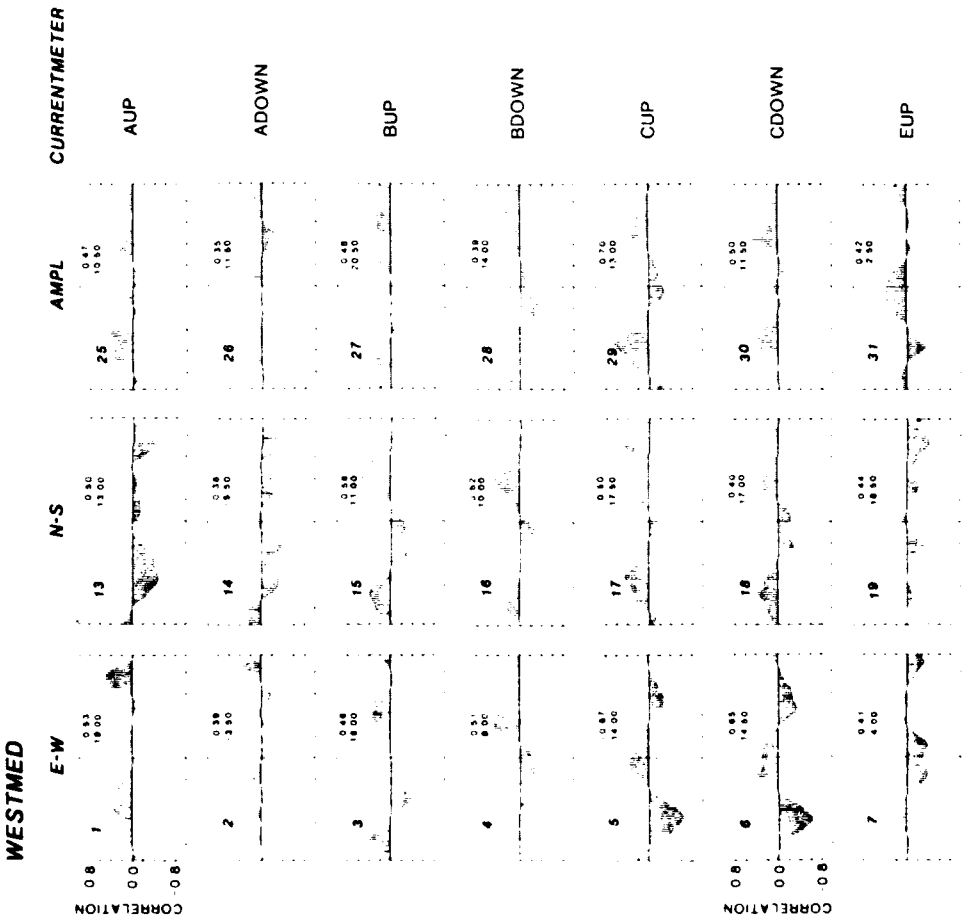
WESTMED
E-W
N-S
AMPL
CURRENTMETER
AUP
ADOWN
BUP
BDOWN
CUP
CDOWN
EUP
CORRELATION
CORRELATION

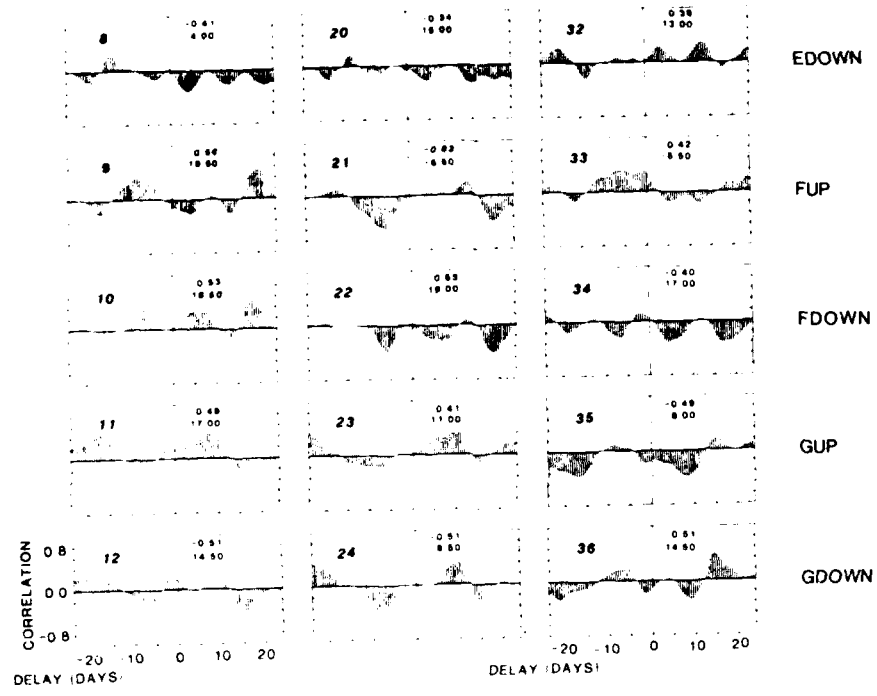

Fig. 49. Cross-correlation between current and average atmospheric pressure over western Mediterranean Sea (WESTMED). Delay, in days, signifies the shift of current meter data relative to the pressure. Current meters are identified on the right side. UP and DOWN signify the current meter at 300 m and 700 m, respectively. E-W, N-S signify east-west, north-south current velocity components and AMPL is the current speed. Numbers in each graph signify the highest cross-correlation and the corresponding delay in hours.

Fig. 50. Cross correlation between float velocity and average pressure over Alboran Sea (ALBORAN) and western Mediterranean Sea (WESTMED). Delay, in days, signifies the shift of float data relative to the pressure. Floats are identified on the right side by number. E-W, N-S signify the east-west and north-south float velocity components and AMPL is the float speed. Numbers in each graph signify the highest cross-correlation and corresponding delay in hours.

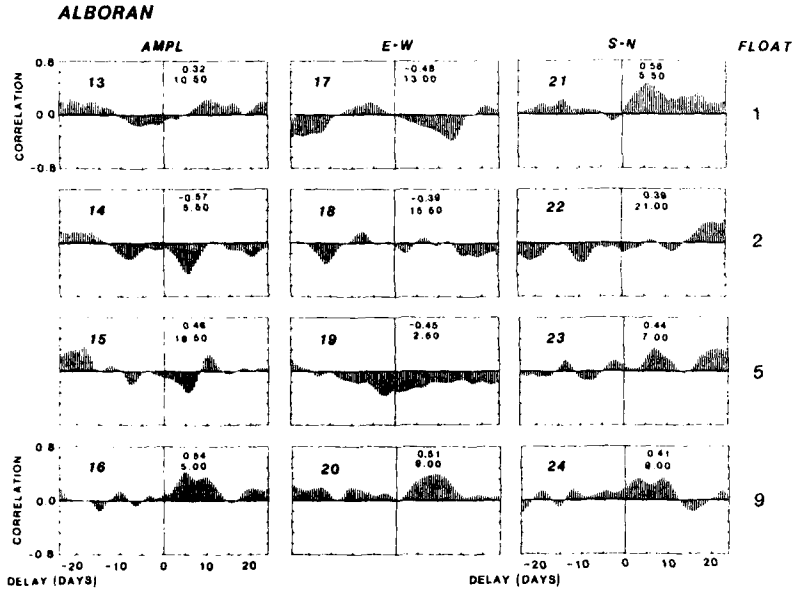
ALBORAN
AMPL
E-W
S-N
FLOAT
CORRELATION
0.8
0.0
-0.8
13
0.32
10.50
17
-0.48
13.00
21
0.56
5.50
1
14
-0.57
5.50
18
-0.39
15.50
22
0.39
21.00
2
15
0.46
18.50
19
-0.45
2.50
23
0.44
7.00
5
16
0.64
5.00
20
0.51
9.00
24
0.41
8.00
9
-20
-10
0
10
20
DELAY (DAYS)

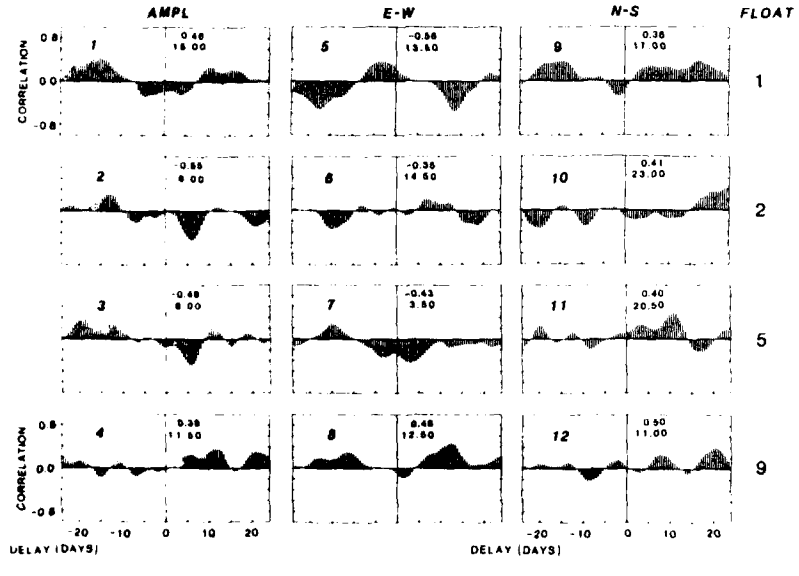
WESTMED
AMPL
E-W
N-S
FLOAT
CORRELATION
0.8
0.0
-0.8
1
0.46
15.00
5
-0.56
13.50
9
0.36
17.00
1
2
0.55
8.00
6
-0.35
14.50
10
0.41
23.00
2
3
-0.48
8.00
7
-0.43
3.50
11
0.40
20.50
5
4
0.38
11.50
8
0.48
12.50
12
0.50
11.00
9
-20
-10
0
10
20
DELAY (DAYS)

Fig. 51. Cross-correlation between float position and average atmospheric pressure over Alboran Sea (ALBORAN) and western Mediterranean Sea (WESTMED). [Delay, in days, signifies the shift of float position data relative to the pressure. Floats are identified on the right side by number. E-W/POS, N-S/POS signify position in east-west or north-south direction, respectively, AMPL/POS is the change in amplitude of position. Numbers in each group signify the highest cross-correlation and the corresponding delay in hours.]

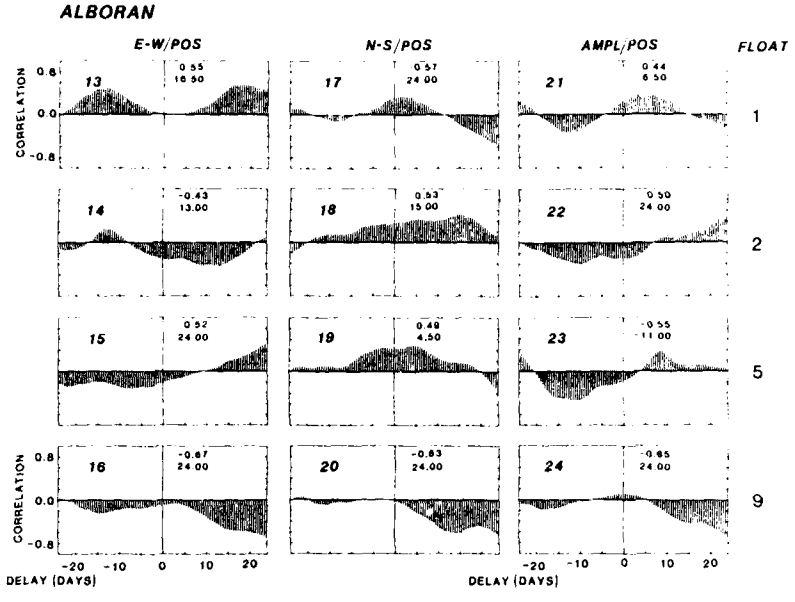
ALBORAN
E-W/POS
N-S/POS
AMPL/POS
FLOAT
CORRELATION
0.8
0.0
-0.8
13
0.55
16.50
17
0.57
24.00
21
0.44
6.50
1
14
-0.43
13.00
18
0.53
15.00
22
0.50
24.00
2
15
0.52
24.00
19
0.49
4.50
23
-0.55
11.00
5
16
-0.67
24.00
20
-0.63
24.00
24
-0.65
24.00
9
-20 -10 0 10 20
DELAY (DAYS)

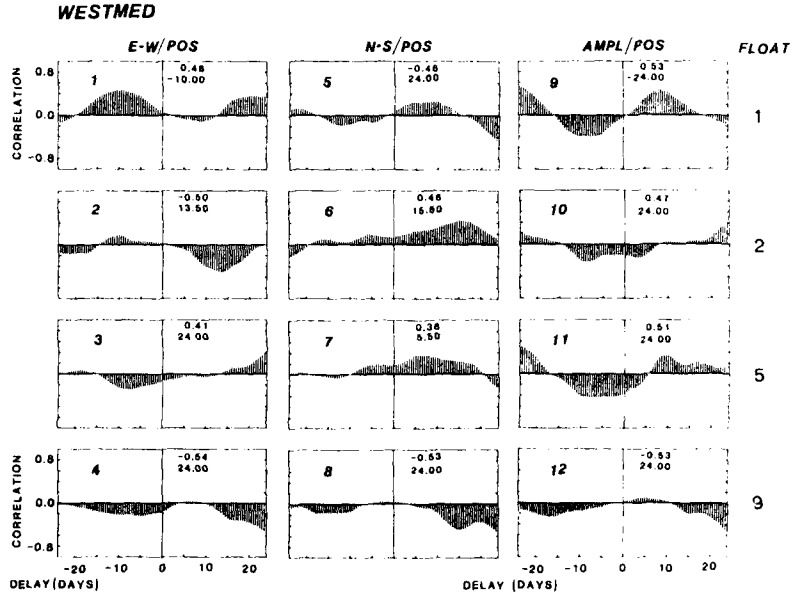
WESTMED
E-W/POS
N-S/POS
AMPL/POS
FLOAT
CORRELATION
0.8
0.0
-0.8
1
-0.48
-10.00
5
-0.48
24.00
9
0.53
-24.00
1
2
-0.50
13.50
6
0.48
15.50
10
0.47
24.00
2
3
0.41
24.00
7
0.36
5.50
11
0.51
24.00
5
4
-0.54
24.00
8
-0.63
24.00
12
-0.53
24.00
9
-20 -10 0 10 20
DELAY (DAYS)

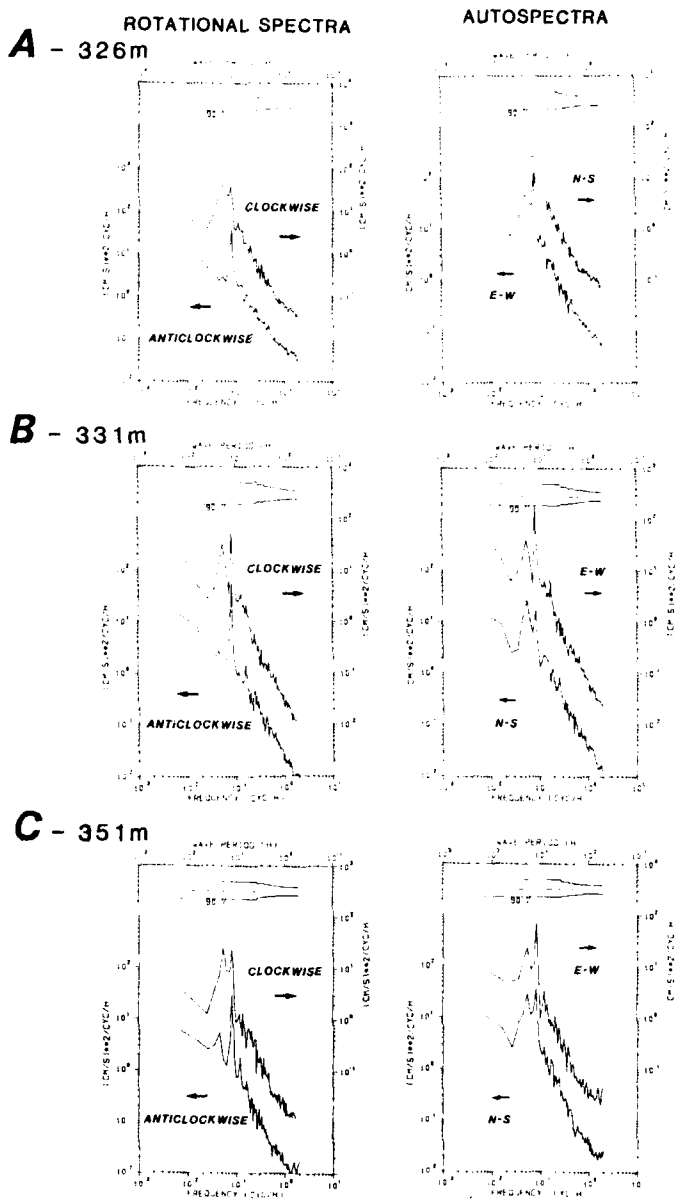

Fig. 52. High-frequency spectra of all current meter data. [Rotational spectra and autospectra for each current meter are identified by mooring and depth. 90% confidence level of gaussian distribution is shown. Wave periods are in hours.]

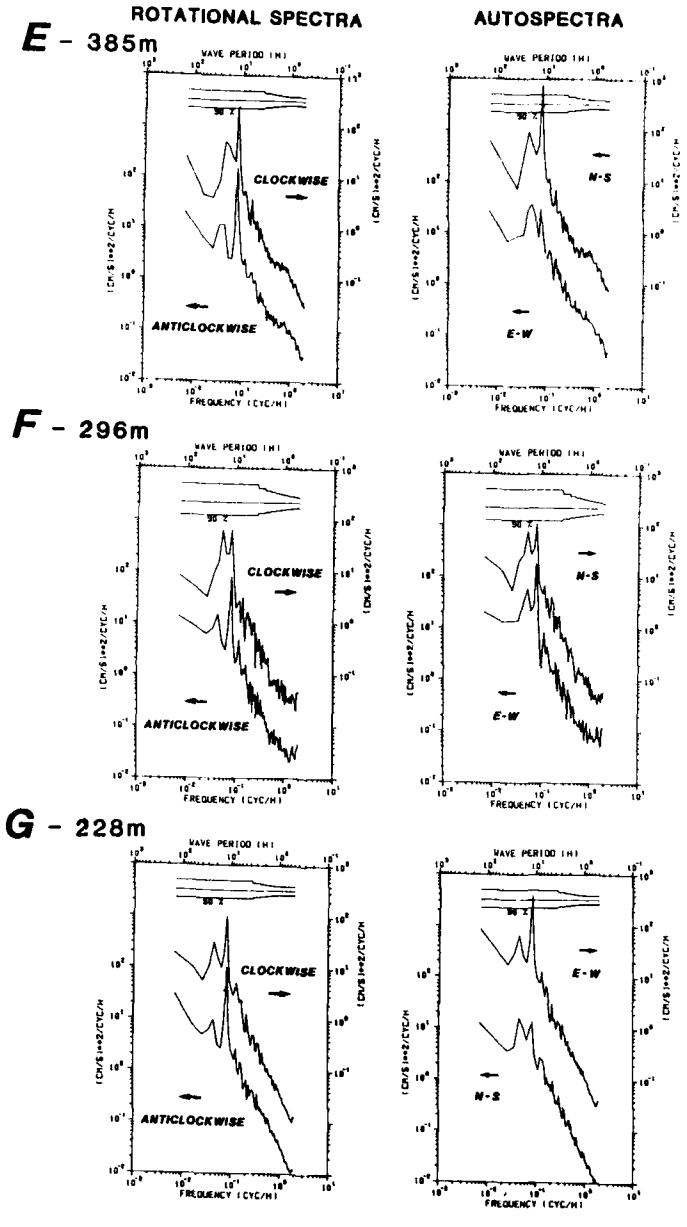

Fig. 52 – continuation 1.

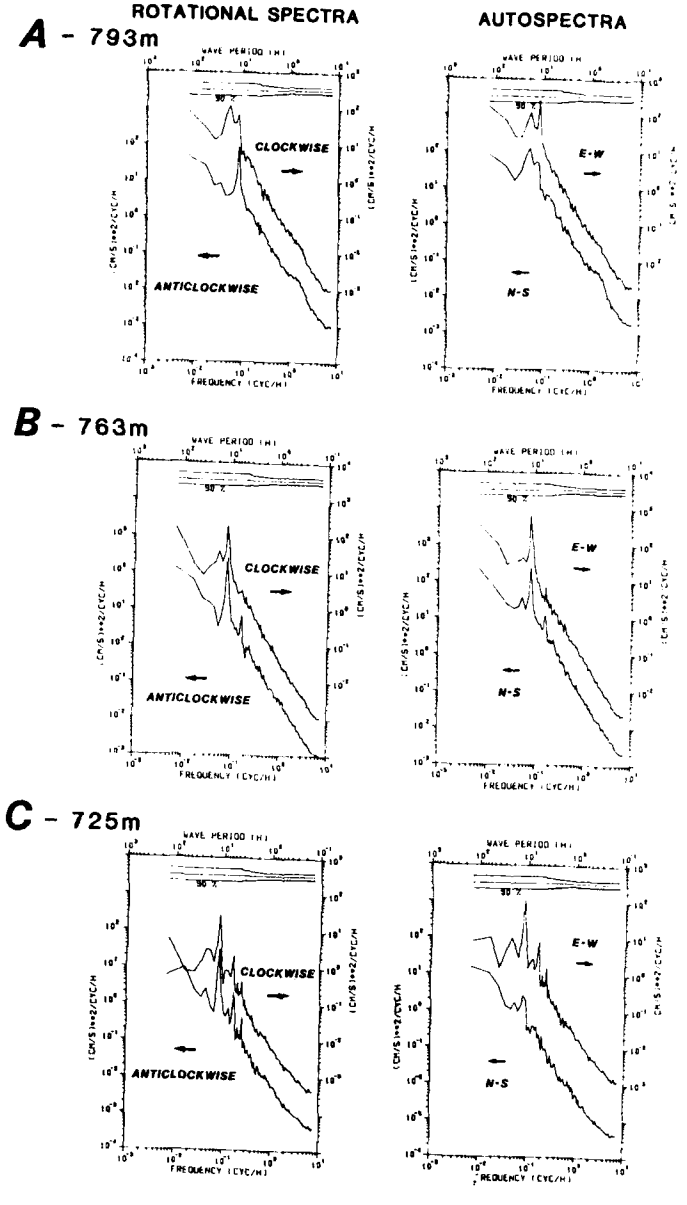

Fig. 52 – continuation 2.

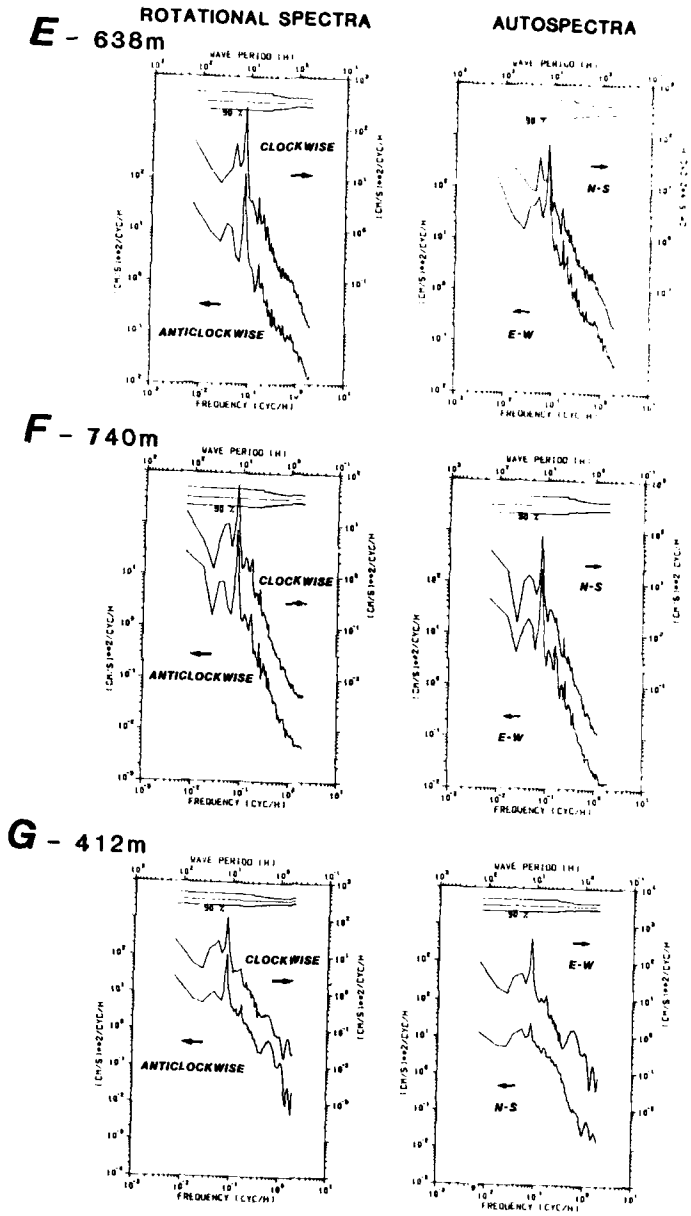

Fig. 52 – continuation 3.

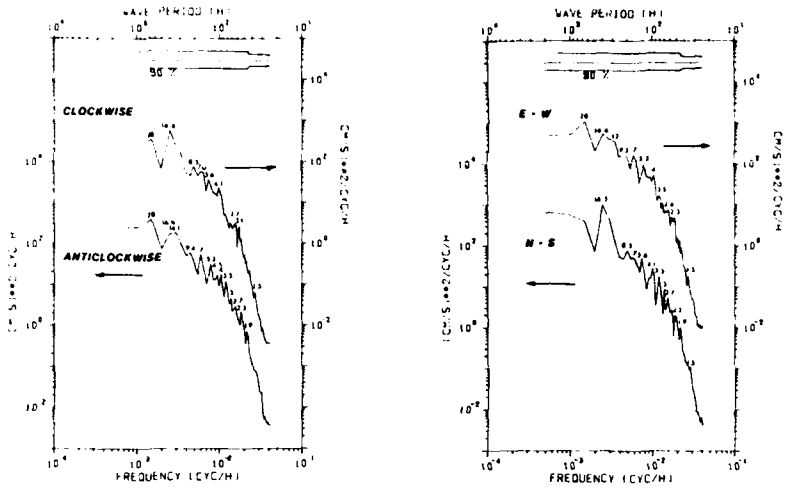

Fig. 53. Low-frequency current meter spectra. [Rotational spectra and autospectra were obtained by averaging of all individual current meter spectra. 90% confidence level of gaussian distribution is shown. Numbers near peaks signify the periods in days.]

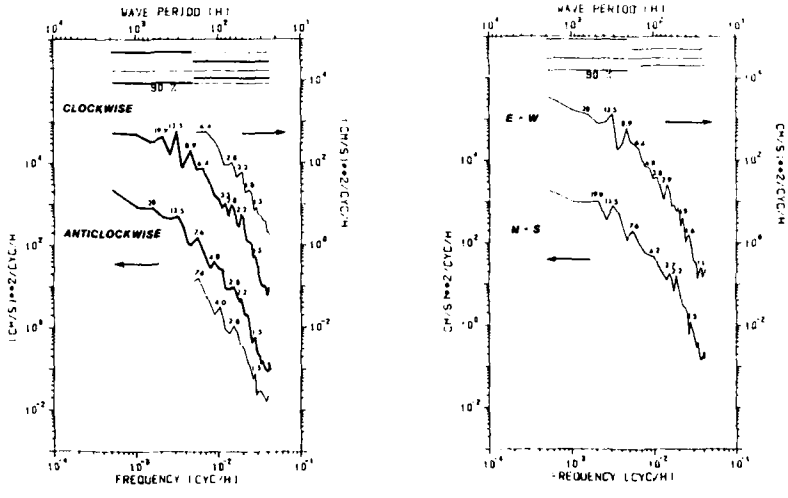

Fig. 54. Low-frequency float spectra. [Rotational spectra and autospectra were obtained by averaging of all individual float spectra. Numbers near peaks signify the periods in days. Thin-line rotational spectra were created by averaging the data from four long-deployed floats. Their scales are shifted relative to total rotational spectra one order up for clockwise and one order down for anticlockwise and their confidence level is the larger one.]

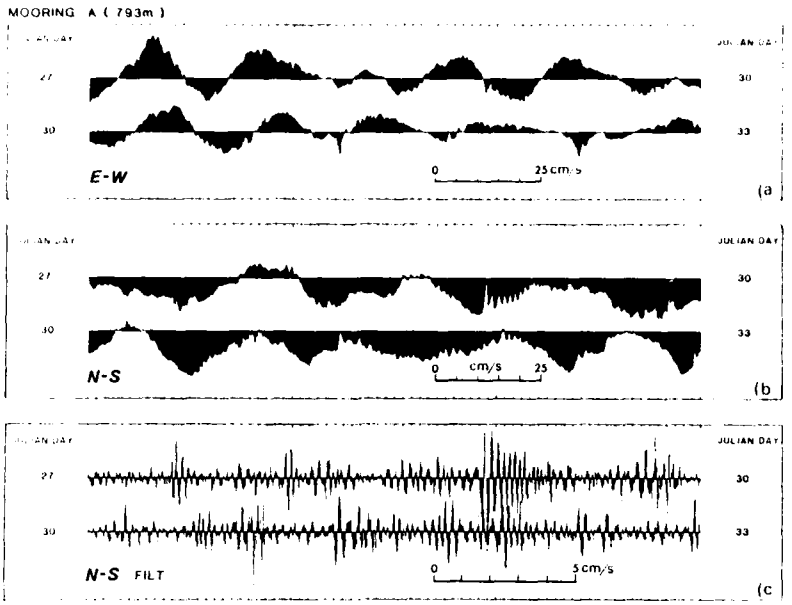

Fig. 55. Train of internal nonlinear waves (solitons) in the southern Alboran Sea. [Position A and depth of 763 m. Superimposed on tidal variation is the high frequency nonlinear wave. E-W, N-S signify the velocity components with the eastward and northward direction positive-up. N-S FILT represents high-pass filtered N-S component.]

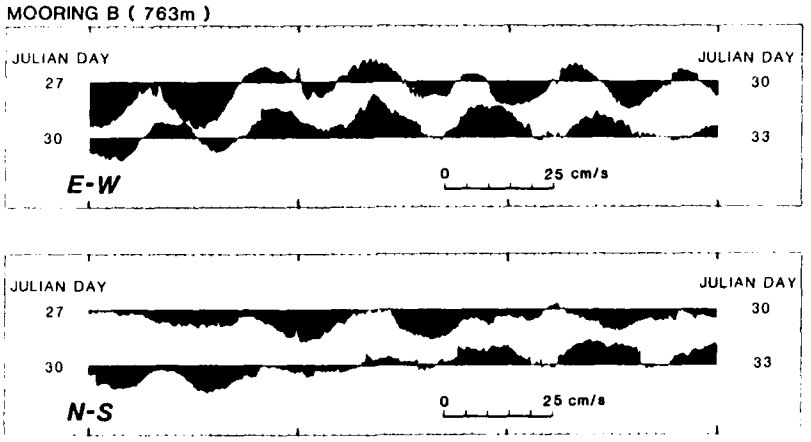

Fig. 56. Train of internal nonlinear waves (solitons) in southern Alboran Sea. [Position B and depth of 763 m. Signal of nonlinear waves is superimposed on tidal variation. E-W, N-S signify the velocity components with the eastward and northward direction positive-up.]

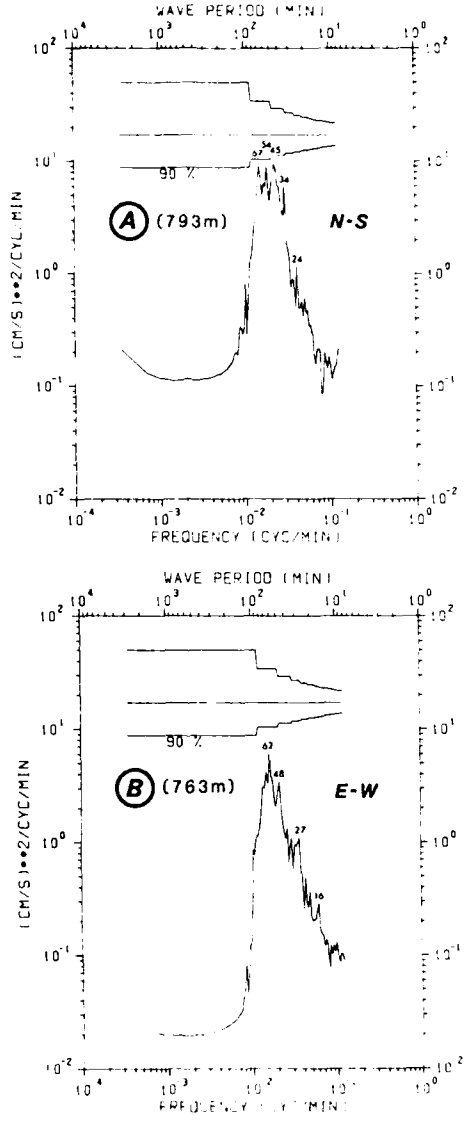

Fig. 57. Spectra of nonlinear wavetrains. [Spectra of the high-pass filtered data for (a) north-south component of velocity at mooring A and depth of 763 m; (b) east-west component of velocity at mooring B and depth of 763 m. The 90% confidence level is shown. Numbers near peaks signify the period in minutes.]

Initial Distribution for SM-195

Ministries of Defence	
JSPHQ Belgium	2
DND Canada	10
CHOD Denmark	8
MOD France	8
MOD Germany	15
MOD Greece	11
MOD Italy	10
MOD Netherlands	12
CHOD Norway	10
MOD Portugal	2
MOD Spain	2
MOD Turkey	5
MOD UK	20
SECDEF US	68
NATO Authorities	
Defence Planning Committee	3
NAMILCOM	2
SACLANT	10
SACLANTREPEUR	1
CINCWESTLANT/ COMOCEANLANT	1
COMSTRIKFLTANT	1
CINCIBERLANT	1
CINCEASTLANT	1
COMSUBACLANT	1
COMMAIREASTLANT	1
SACEUR	2
CINCNORTH	1
CINCSOUTH	1
COMNAVSOUTH	1
COMSTRIKFORSOUTH	1
COMEDCENT	1
COMMARAIRMED	1
CINCHAN	3
SCNR for SACLANTCEN	
SCNR Belgium	1
SCNR Canada	1
SCNR Denmark	1
SCNR Germany	1
SCNR Greece	1
SCNR Italy	1
SCNR Netherlands	1
SCNR Norway	1
SCNR Portugal	1
SCNR Turkey	1
SCNR UK	1
SCNR US	2
SECGEN Rep. SCNR	1
NAMILCOM Rep. SCNR	1
National Liaison Officers	
NLO Canada	1
NLO Denmark	1
NLO Germany	1
NLO Italy	1
NLO UK	1
NLO US	1
NLR to SACLANT	
NLR Belgium	1
NLR Canada	1
NLR Denmark	1
NLR Germany	1
NLR Greece	1
NLR Italy	1
NLR Netherlands	1
NLR Norway	1
NLR Portugal	1
NLR Turkey	1
NLR UK	1
Total external distribution	248
SACLANTCEN Library	10
Stock	22
Total number of copies	280

END

DATE
FILMED

3 88